

Seasonal and interannual global surface mass variations from multisatellite geodetic data

Xiaoping Wu,¹ Michael B. Heflin,¹ Erik R. Ivins,¹ and Ichiro Fukumori¹

Received 10 October 2005; revised 9 March 2006; accepted 5 May 2006; published 6 September 2006.

[1] Monthly global surface mass distribution changes are estimated in the spherical harmonic domain with a complete spectrum up to degree and order 50. The estimates are derived by inverting GPS displacement series measured at roughly 450 continuously tracking sites and ocean bottom pressure (OBP) estimates of a data assimilated ocean circulation model from 1993 to 2004. The inversion uses a hybrid estimator after singular value decomposition of the normalized measurement equations with reduced reliance on a priori spectral information. The results are then compared and combined with Gravity Recovery and Climate Experiment (GRACE) gravity data to provide enhanced spectral and geographic coverage. High fidelity degree-1 surface mass variation coefficients are recovered, corresponding to equivalent geocenter motion with better than 0.5 mm annual amplitude precisions in all three components. A clear annual surface mass cycle occurs in both GPS/OBP- and GRACE-derived results. There is very good agreement among the low-degree spherical harmonic coefficients and in global geographic pattern but with significant regional differences in amplitudes. Annual variations of average mass over the global oceans, Antarctica, and Greenland are then derived. Total surface mass over both Antarctica and Greenland peak in their respective summers due to increased atmospheric mass. Large interannual variations have also been found involving several continents in the 11-year GPS/OBP solution. The patterns of variation suggest that the recent satellite laser ranging (SLR) observation of a reversal in trend of the Earth's oblateness may be largely an interannual surface mass cycle with considerable contribution from the northern continents.

Citation: Wu, X., M. B. Heflin, E. R. Ivins, and I. Fukumori (2006), Seasonal and interannual global surface mass variations from multisatellite geodetic data, *J. Geophys. Res.*, *111*, B09401, doi:10.1029/2005JB004100.

1. Introduction

[2] Driven by external and internal forcing, the Earth's surface layer undergoes constant changes with a multitude of spatiotemporal scales. An important indicator and measure of the change dynamics in the atmosphere, hydrosphere, and cryosphere is the significant horizontal water mass transport through precipitation, evapotranspiration, and runoff. Surface mass variations such as sea level change, ice mass imbalance, and varying soil moisture content also have important habitat, agricultural, and hazard implications to the world community and can serve as feedback mechanisms to alter climate forcing.

[3] Surface mass variations leave several distinct geodetic signatures. In the last few years, significant advances in satellite tracking technologies have revolutionized geodetic measurements of surface mass variation in coverage, accuracy, and resolution, with several global monitoring capabilities emerging. This brings global geodesy to the forefront of climate change research. The Earth's external

gravity field changes as a result of direct gravitational attraction of the moving mass and indirect effect of mass redistribution inside the Earth due to surface load induced deformation. The low-degree zonal spherical harmonic components of the gravity change due to surface mass variations have been observed in the last three decades [e.g., Yoder *et al.*, 1983; Ivins *et al.*, 1993; Cheng and Tapley, 1999, 2004; Cox and Chao, 2002; Dickey *et al.*, 2002; Hughes and Stepanov, 2004]. The most notable recent progress is the successful launching and operation of the Gravity Recovery and Climate Experiment (GRACE) satellite-to-satellite microwave tracking gravity mission [Tapley *et al.*, 2004]. This marks an important transition from component or local measurements to global high resolution and accuracy monitoring of the mass transport process in the Earth system [Wahr *et al.*, 2004]. Satellite gradiometry and laser interferometric satellite-to-satellite tracking missions and technologies are also under study for follow-on gravity missions [e.g., Bouman *et al.*, 2004; Bender *et al.*, 2003]. The redistributed surface mass also loads the solid Earth resulting in crustal deformation that can be measured by the continuous tracking Global Positioning System (GPS) network with increasing global coverage and density (about 1000 current sites), and by the emerging interferometric synthetic aperture radar (InSAR)

¹Jet Propulsion Laboratory, California Institute of Technology, Pasadena, California, USA.

technology [e.g., *van Dam et al.*, 1997; *Galloway et al.*, 1998; *Wu et al.*, 2003]. The degree-1 spherical harmonic components of the surface mass variation with the largest spatial scale cause the center of mass (CM) of the total Earth system to shift with respect to the center of figure (CF) of the solid Earth surface [*Farrell*, 1972; *Trupin et al.*, 1992; *Dong et al.*, 1997; *Chen et al.*, 1999]. This phenomenon is often referred as geocenter motion and can be measured by tracking satellite motion from a global geodetic network, or inferred from the measured surface deformation [e.g., *Eanes et al.*, 1997; *Ray*, 1999; *Bouille et al.*, 2000; *Blewitt et al.*, 2001; *Wu et al.*, 2002, 2003; *Blewitt and Clarke*, 2003]. Over the oceans, more than a decade of satellite altimetry has provided a rich data set of sea surface height (SSH) measurements over a large latitude band (from 66°S to 66°N). These and other data have been assimilated in dynamic oceanic general circulation models (GCM) with atmospheric forcing except pressure loading to infer for oceanic states including surface mass variations in terms of ocean bottom pressure (OBP) [*Fukumori et al.*, 1999]. The laser altimeters on the ICESat have also demonstrated the technology potential and yielded useful elevation data.

[4] In this paper, we will focus on the seasonal and interannual surface mass variations. The GRACE mission has released 21 quasi-monthly gravity fields spanning over more than 2 years (due to global coverage requirement and data availability, gravity solutions are sometimes derived using tracking data acquired during periods of less than a full month or across monthly boundaries). Obviously, such high resolution and accuracy time-variable gravity fields have no other external global gravity comparison. However, the combination of global GPS data and the assimilated model OBP results have the potential to provide a complete and independent global measure of surface mass variations. If time-variable gravity and crustal deformation at the seasonal scale are both caused by surface mass variations, then comparison between GPS/OBP- and GRACE-derived surface mass variations can cross validate the crustal deformation and time-variable gravity data as well as their respective uncertainty estimates. Moreover, time-variable gravity fields have been attributed largely on theoretical grounds to horizontal mass transport on the Earth's surface layers except for those with very long timescales [e.g., *Chao*, 2005]. Comparison of the two independent techniques thus can add observational evidence to support such a hypothesis and help identify or confirm the sources of change in the measured geodetic quantities [e.g., *Chambers et al.*, 2004; *Kusche and Schrama*, 2005].

[5] Also, the GRACE mission and the GPS/OBP data are complementary to each other. Despite the impressive progress in the respective technologies, currently no single technique can provide complete spatiotemporal coverage with high resolution and accuracy. For example, spherical harmonic expansion of the surface mass variations begins with degree-1 components with the longest wavelength. However, since the coordinate origin of the GRACE data system is defined as the center of mass of the total Earth system, the degree-1 gravity components vanish. This effectively separates degree-1 surface mass variations from the gravity fields and leaves three distinct global-scale spherical harmonic gaps in the incremental surface mass spectrum. These gaps can be filled through measurements of

geocenter motion, which, by the above definition, is independent from the time-variable gravity field. Experimental geocenter motion results have been reported using satellite laser ranging (SLR) data (see above) which are considered more reliable than other techniques. The primary difficulty with this technique is the sparse and shrinking SLR tracking network. What is measured by the direct satellite-tracking method is relative motion between CM and center of (the tracking) network (CN), which for a sparse network may be significantly different from that between CM and CF and thus degree-1 surface mass variations [*Wu et al.*, 2002]. On the other hand, GPS/OBP data coverage over polar areas and southern continents remains poor. In addition, the OBP model lacks information on the total incremental mass over the oceans due to the Boussinesq approximation [e.g., *Greatbatch*, 1994] and absence of water mass input to or output from the oceanic system.

[6] The combination of these data types can therefore lead to better accuracy, resolution, geographic and spectral coverage, including potentially more robust estimation of degree-1 surface mass variations. The heterogeneous GPS site distribution presents a further challenge for inversion in the spherical harmonic domain. A low degree truncation discards a large amount of information over densely covered areas, whereas a high degree truncation results in a severely ill-posed problem. In this paper, the ill-posed problem will be solved by a hybrid form of least squares estimator (LSE) and best linear estimator (BLE) that seeks reduced aid of a priori model under the platform of singular value decomposition (SVD). On the interannual scale, the GPS/OBP data span more than 11 years with increasing GPS site coverage. These have not been fully explored before. The reported SLR J_2 reversal occurred during this time period. The better global distribution of GPS/OBP data may be able to corroborate the result and provide more information about this phenomenon including geographic sources and details.

[7] Seasonal and interannual surface mass variations and their geodetic signatures will be discussed briefly in section 2. We then invert for seasonal global surface mass variations in spherical harmonic domain (degree 1 to 50) and their geographical representations from concurrent GPS/OBP and GRACE data separately and in combination. The spherical harmonic and geographic results including mean mass variations over global oceans, Antarctica and Greenland with and without atmospheric contributions will be compared and discussed. We will also present GPS/OBP inverted results from 1993 to 2004 including interannual variations.

2. Surface Mass Variations and Their Geodetic Signatures

[8] At current stage of investigation, vertical mass distribution and transport are ignored and the Earth's changing atmosphere, hydrosphere, and cryosphere are modeled collectively as an infinitesimal thin layer on a spherical surface [e.g., *Wahr et al.*, 1998]. Mass variations above the solid Earth will be restricted to this surface as changes in surface mass density or thickness of water equivalent. Mass redistribution inside the solid Earth is induced as a result of the surface load. Compatible with gravity convention and

historical data, in the terrestrial reference frame with coordinate origin defined at the geometric center of the spherical surface, the incremental surface density referenced with respect to a particular epoch can be expressed as a function of time t , colatitude θ , and longitude ϕ , by a sum of spherical harmonic series:

$$\begin{aligned} \Delta M(\theta, \phi, t) &= \rho_w \Delta h(\theta, \phi, t) \\ &= \sum_{n=1}^{\infty} \sum_{m=0}^n \sum_{q=c,s} \Delta M_{nmq}(t) Y_{nmq}(\theta, \phi), \end{aligned} \quad (1)$$

where $\rho_w = 1.025 \text{ kg m}^{-3}$ is the reference density of water, h is the thickness of water equivalent. $Y_{nmq}(\theta, \phi)$ is the real-valued spherical harmonic function normalized under geodetic convention [e.g., *Lambeck, 1988*]. From now on, the independent variables of various functions will be conveniently dropped from equations when no confusion can arise. Also, the same summations over nmq as appeared in (1) will be simplified as \sum_{nmq} .

[9] Over the oceanic area, an equivalent expression of surface mass density is the bottom pressure:

$$\Delta P = g \Delta MO(\theta, \phi), \quad (2)$$

where g is the normal gravity at the surface of the Earth, and O is the ocean function such that $O = 1$ over the oceans and $O = 0$ over the land.

[10] At seasonal and interannual timescales, the Earth deforms largely as a spherically symmetric elastic body. In the reference frame with origin fixed at center of mass of the deformed solid Earth (CE), the external gravitational potential will change resulting from the direct surface mass attraction and load-induced deformation and mass redistribution. The potential field is often described by the geoid, which is an equipotential surface coinciding with the mean sea level at a particular epoch. According to Brun's formula, changes in geoidal heights above the Earth's reference ellipsoid N will be proportional to changes in the external potential at the Earth's surface W and is related to the incremental surface mass:

$$\begin{aligned} \Delta N &= \frac{\Delta W}{g} = \sum_{nmq} \Delta N_{nmq} Y_{nmq} \\ \Delta N_{nmq} &= \frac{4\pi a^3}{M_E} \frac{1 + k'_n}{2n + 1} \Delta M_{nmq}, \end{aligned} \quad (3)$$

where a is Earth's radius, M_E is the Earth's mass, and k'_n is the potential load Love number.

[11] The variation of load mass causes the solid Earth surface to deform resulting in a vector displacement field [e.g., *Farrell, 1972; Wilhelm, 1986*]:

$$\begin{aligned} \mathbf{s} &= \frac{4\pi a^3}{M_E} \sum_{nmq} \frac{\Delta M_{nmq}}{2n + 1} [h'_n Y_{nmq} \hat{\mathbf{e}}_r + l'_n \partial_\theta Y_{nmq} \hat{\mathbf{e}}_\theta \\ &\quad + l'_n \frac{1}{\sin \theta} \partial_\phi Y_{nmq} \hat{\mathbf{e}}_\phi], \end{aligned} \quad (4)$$

where h'_n and l'_n are the vertical and horizontal surface displacement load Love numbers, respectively, and $\hat{\mathbf{e}}$ is the unit spherical coordinate vector.

[12] The degree-1 surface mass load also causes the center of mass (CM) of the entire Earth system and the center of figure (CF) of the solid Earth surface to shift with respect to each other, commonly referred as geocenter motion [*Trupin et al., 1992*]:

$$\begin{aligned} \mathbf{r}_{\text{cm}} - \mathbf{r}_{\text{cf}} &= \frac{4\pi}{\sqrt{3}} \frac{a^3}{M_E} \left(1 - \frac{h'_1 + 2l'_1}{3} \right) \\ &\quad \cdot (\Delta M_{11c} \hat{\mathbf{e}}_x + \Delta M_{11s} \hat{\mathbf{e}}_y + \Delta M_{10c} \hat{\mathbf{e}}_z). \end{aligned} \quad (5)$$

This definition of geocenter motion is mathematically convenient since such motion has a one-to-one correspondence with degree-1 surface load coefficients. However, its global integral nature dictates that it can only be approximated by ground networks which will never be infinitely dense. Rigorously, direct satellite tracking measures geocenter (CM) motion with respect to the center of network (CN). The motion between CF and CN can reach the level of 1 mm for a typical global SLR network, and much smaller for larger global GPS networks [*Wu et al., 2002*].

[13] If the reference frame is chosen such that the coordinate origin is defined as CM in the case of the GRACE data system, then degree-1 gravity and geoid components all vanish. However, the degree-1 mass terms on the surface of the Earth do not. Currently, all analysis centers of the GRACE project use either a subset of the global GPS network or the point-positioning strategy using GPS orbits determined by the International GPS Service (IGS). The IGS orbits and ground station coordinates are defined in the International Terrestrial Reference Frame (ITRF). At the seasonal to interannual scales, the origins of these frames are actually tied with CN rather than CM. Inconsistency can also result from any fiducial approach that assumes linear relative ground station movements. The most notable consequence of the present processing strategy, however, is the lack of geocenter motion information or degree-1 surface mass variations.

[14] Another subtle point is that the spherical harmonic series in (1) starts from $n = 1$, since the total mass in the surface layer is assumed to be conserved and thus $\Delta M_{00c} = 0$. However, mass exchanges do occur among the components of the surface layer of the Earth, such as the atmosphere, oceans, ice sheets, and land. The total mass in each component is usually not conserved. Therefore, when mass variations are considered separately for the components, their spherical harmonic expansion should start from $n = 0$ rather than $n = 1$ as appears in (1) [e.g., *Gross et al., 2004*]. For example, when atmospheric mass is considered separately or when it is removed from the total surface mass, $\Delta M_{00c}(t)$ should be retained in the spherical harmonic series.

3. Inverse and Data Combination: Methodology

3.1. Measurement Models

[15] Although GPS measurements contain certain absolute information tying the ground and space segments to physical or celestial reference frames, many components of the link are weak. For example, currently, direct GPS geocenter motion determination has large uncertainties. This

information thus will not be used in our study. The scale expansion of the ground network can either be estimated directly using the metric scale defined by the GPS system or fixed to the ITRF linear site motion model. Historically, the GPS metric scale has shown large daily to monthly fluctuations. GPS metric scale is also affected by the uncertainties in transmitter and receiver phase center knowledge, which has received considerable attention recently. These have led many analysis centers to take a seven-parameter network transformation approach to realign the free-network solution (after correcting for solid Earth tides, ocean tide loading, and solid Earth pole tides) to the ITRF reference frame with the scale defined by ITRF coordinate model determined with SLR and very long baseline interferometry techniques [Heflin *et al.*, 1992]. However, the ITRF coordinates assume a linear model and do not allow seasonal or interannual variations. As noted by Lavalée *et al.* [2003] and Tregoning and van Dam [2005], such omission is inconsistent with our theme of subinterannual surface mass variations and load-induced deformation and will introduce a scale error in the coordinate solution and consequently an erroneous network expansion. When coupled with a north-south hemispherical asymmetry in GPS site distribution, the scale error can alias significantly into estimated geocenter motion along the z axis if GPS displacements derived in such a way are inverted. The residual translation and rotation among the daily coordinate solutions largely reflect fluctuations resulting from changes in network configuration or data processing and contain no geophysical information.

[16] The above reasoning has led us to take the geophysically significant intrinsic deformation (or projected deformation) as GPS measurements in the inverse problem with the following reference frame invariant form:

$$\bar{\mathbf{s}} = \left(\mathbf{I} - \mathbf{A}(\mathbf{A}^T \mathbf{A})^{-1} \mathbf{A}^T \right) \mathbf{s}, \quad (6)$$

where \mathbf{A} is the partial derivative matrix used in the seven-parameter network transformation approach [e.g., Blewitt *et al.*, 1992], and \mathbf{I} is the identity matrix. Physically, $\bar{\mathbf{s}}$ is equivalent to the displacement vector with respect to the center of network and mean axes without scale information. The observation equation is constructed correspondingly when (4) is substituted into (6).

[17] In addition to load-induced deformation, the ground GPS measurements are also sensitive to other geophysical phenomena. To reduce such sensitivities and enhance data quality, a site selection and data-editing procedure is applied to a network of more than 900 globally distributed continuous GPS sites. The criteria are that sites should contain data in March 2004, have more than 2 years of tracking history, and contain at least 6 months of data during the 18 GRACE quasi-months. In addition, known problematic sites and sites associated with aquifer activity in California [Argus *et al.*, 2005] are removed from the study. Data with unusually large monthly or quasi-monthly (hereafter referred simply as quasi-monthly) standard deviations and significantly affected by large earthquakes are also rejected. Consequently, about 450 sites are chosen in our study.

[18] The OBP estimates are based on a data assimilated ocean general circulation model of the Consortium for

Estimating the Circulation and Climate of the Ocean (ECCO) [Stammer *et al.*, 2002]. Sea level observations by satellite altimetry and in situ temperature profiles are assimilated into a near global ocean circulation model using an approximate Kalman filter [Fukumori *et al.*, 1999]. The model extends from 73°S to 73°N and employs a 1° grid except in the tropics where the meridional resolution is gradually increased from 20° of the equator to a 0°3 resolution within 10° of the equator. Estimates from this model are available from 1993 to present. The current study employs 12-hourly OBP estimates from 1993 to 2004. The model employs the Boussinesq approximation that conserves volume instead of mass. This situation is corrected by removing the net global mass fluctuations of the oceans as if it were uniformly distributed [Greatbatch, 1994]. On the seasonal to interannual timescales, the response of the ocean to atmospheric pressure forcing will largely be that of an inverse barometer. The GCM is forced by atmospheric winds, heat and freshwater fluxes but not by atmospheric pressure. Freshwater fluxes are implemented as virtual salt fluxes; the model does not allow net in or out flow of water mass to or from the oceanic system. As a result, the OBP model is biased by the sum of spatial mean atmospheric pressure and water exchange with land. To overcome this difficulty in the model, we will treat the quasi-monthly averaged OBP records P_a on a 5° × 5° grid (in rough accord with our spherical harmonic truncation at degree-50 having a wavelength of 800 km) as pseudo point observations with a constant bias $P_0(t)$ to be estimated each quasi-month along with surface mass variations:

$$\Delta P_a(\theta, \phi, t) = O \left[\Delta P_0(t) + g \sum_{nmq} \Delta M_{nmq} Y_{nmq} \right]. \quad (7)$$

Another inconsistency exists between the pseudo OBP data and the GPS data described above. The GPS data are not corrected for loading effect of the oceanic pole tides. Their inversion theoretically should lead to the surface mass variation including that due to the oceanic pole tide, despite their sparse distribution over the oceans. The assimilated OBP model on the other hand does not contain the oceanic pole tide signature. To be consistent with the released GRACE data which also contain the oceanic pole tide signature (J. M. Wahr and S. V. Bettadpur, private communications, 2004), we add the mass-conserving equilibrium ocean floor pole tide [Lambeck, 1988] to the OBP model using Earth orientation parameter values determined by the International Earth Rotation and Reference Systems Service.

[19] The GRACE level 2 products used in this paper contain 18 sets of geoid coefficients ($n \geq 2$) and their calibrated uncertainties spanning from April 2002 to March 2004. The geoid coefficients have been corrected by the dealiasing products based on an atmospheric model and a barotropic ocean model. While the dealiasing effort effectively removes high-frequency effects in the tracking data, the barotropic model is less accurate over the period of a month. To reconstruct the observed geoid field including the contributions of oceans and atmosphere, the mean dealiasing model over each data period is added back to the corrected field. The covered time in the data sets is also not

homogeneous. In our study, the time tag is accurately tracked and averaged to correspond to the central epoch of each data set period.

[20] To focus on seasonal and interannual variations, and to avoid complications of secular phenomena such as plate motion, postglacial rebound and other tectonic activities, linear trends are first estimated and removed from the daily point-positioned [Zumberge *et al.*, 1997] GPS coordinates in the ITRF reference frame [Heflin *et al.*, 2002], 12-hour OBP values, and GRACE gravity coefficients. The detrended GPS and OBP time series are then averaged to form incremental concurrent quasi-monthly means (with same days in the gravity solutions) for the 18 GRACE quasi-months and incremental monthly means between January 1993 and March 2004 after deducting values for March 2004. The quasi-monthly averaged GPS displacements are then further projected for use in data inversion.

[21] As a result of point-positioning strategy, only correlations among coordinates of each individual site are available. For spherical coordinates, these are very small. The effects of correlations among GRACE spherical harmonic coefficients are also found to be small for our purposes. Therefore only the diagonal components of the covariance matrices for GPS and GRACE data are used in this study. A uniform quasi-monthly uncertainty of 1.7 cm is assumed for the water-equivalent thickness uncertainty σ_h for each oceanic grid cell, and $\sigma_p = \rho_w g \sigma_h$ (Topex/Poseidon has a 2 cm 10-day $1^\circ \times 1^\circ$ grid uncertainty. To account for additional reference frame related and other errors, we assume the total 10-day uncertainty to be 3 cm, which is likely to have a dominant contribution from spatial-invariant systematic errors. Thus $\sigma_h = 3/\sqrt{3} = 1.7$ cm.) The comparisons with the bottom pressure gauge measurements [Fukumori *et al.*, 1999] tend also to support this level of uncertainty for the assimilated OBP model. The GPS/OBP data will be used to solve for \mathbf{X} , a $k \times 1$ parameter vector containing surface mass density coefficients $\Delta M_{nmq}(t_i)$ and the constant mean oceanic bias $\Delta P_0(t_i)$ for each quasi-month.

3.2. Inverse Formulation

[22] In the spherical harmonic domain, surface mass variation is an infinite series. Certain a priori information is needed in order to obtain a meaningful solution of the coefficients using the GPS/OBP data. A statistical optimal method is the LSE with a priori information. The method, however, relies on the a priori model, which, in this case, is very limited in terms of availability and reliability. Such estimates can be severely contaminated by deficiencies in the model. For example, the existing hydrological models are not well calibrated by actual observations. It is also very difficult to assess their covariances. A robust inversion, therefore, should use as little such a priori information as possible.

[23] A usual approach of harmonic inversion is to truncate the series to certain degree and order and solve for the remaining coefficients. The higher-degree terms, although hopefully small, will alias into and contaminate the low-degree estimates along with data noise. The aliasing effect and total uncertainties of the estimates can be assessed using a priori parameter model and data covariance matrix. This approach has been taken by Wu *et al.* [2003]. The truncation

degree was chosen in an ad hoc and trial and error manner so that the total uncertainties in the estimates are nearly minimized. The advantage of such approach is that once the truncation degree is chosen, although still contaminated by the actual higher degree terms, the estimates are independent of the a priori parameter model. One obvious disadvantage of such approach is the lack of an objective and quantitative criterion in choosing the truncation degree. More seriously, the GPS site distribution is not geographically uniform. In other words, the spatial coverage of the GPS network depends more on other factors such as accessibility and available resources than spherical harmonic wavelength. The truncation degree chosen by Wu *et al.* [2003] is largely dictated by the sparse data coverage over the oceanic area and many southern continents. A large amount of information offered by the dense GPS networks over North America and Eurasia is discarded. If a much higher truncation is taken, the sparse data coverage implies an ill-conditioned observation matrix. This will greatly magnify uncertainties in the solution due to data noise and make the entire harmonic spectrum useless.

[24] To overcome these difficulties, in this paper, we will use a method first proposed by Matsu'ura and Hirata [1982]. After truncating the spherical harmonic series to a sufficiently high degree and order (50 in our case), the quasi-monthly measurement equations of projected GPS and OBP data are combined (for GPS/OBP), and further with that of GRACE data (for GPS/OBP/GRACE), in the following matrix form with the mean time at t_i :

$$\mathbf{L} = \mathbf{H}\mathbf{X} + \Delta, \quad (8)$$

where \mathbf{L} is the $l \times 1$ data vector representing the derived projected GPS site deformation and gridded OBP (plus GRACE geoid coefficients for GPS/OBP/GRACE).

[25] For a priori parameter information, we use National Centers for Environmental Prediction/National Center for Atmospheric Research (NCEP/NCAR) reanalysis products [Kalnay *et al.*, 1996] and assimilated ECCO OBP model to form quasi-monthly time series of combined atmosphere/land/ocean surface density in the spherical harmonic domain up to degree/order 50. A common difficulty in constructing a priori information from a geophysical model is the lack of uncertainty estimates in some of these models, which is also true in our case, and particularly so for the hydrological model with very little data calibration. Combining estimates from different observing systems and models must also contend with representativeness errors of the respective systems that are not entirely obvious. Thus, to be conservative on the reliability of the combined model, the a priori mean for each quasi-monthly parameter is taken to be $\mathbf{X}_0 = \mathbf{0}$. One choice of a priori variance for each spherical harmonic component in any month is the temporal mean square of its time series. To avoid the case of overly tight a priori constraint resulting from severe model underprediction over certain geographic regions, we further take the average of the $2n + 1$ temporal mean squares of degree- n spherical harmonic coefficients as the a priori quasi-monthly variance for every degree- n coefficient:

$$\sigma_n^2 = \frac{1}{2n+1} \sum_{m=0}^n \sum_{q=c,s} \sum_{i=1}^{N_i} \frac{\Delta M_{nmq}^2(t_i)}{N_i}, \quad (9)$$

where N_t is the number of quasi-months in the model. The a priori root variance of the quasi-monthly oceanic bias is taken to be $\sigma_{p_0} = \rho_w g \sigma_{h_0}$, and $\sigma_{h_0} = 10$ cm. In other words, the a priori quasi-monthly water-equivalent mean sea level uncertainty is assumed to be 10 cm. These will be used along with σ_n to form the diagonal a priori covariance matrix Σ_x .

[26] To be applicable to a more general case when $\mathbf{X}_0 \neq \mathbf{0}$, the observation equation (8) can be modified by subtracting $\mathbf{H}\mathbf{X}_0$ on both sides and defining $\Delta_L = \mathbf{L} - \mathbf{H}\mathbf{X}_0$, $\Delta_x = \mathbf{X} - \mathbf{X}_0$ to obtain

$$\Delta_L = \mathbf{H}\Delta_x + \Delta. \quad (10)$$

The data noise covariance and the a priori parameter covariance matrices are then square root decomposed into

$$\Sigma_\Delta = \mathbf{R}_\Delta^{-1} \mathbf{R}_\Delta^{-T}, \Sigma_x = \mathbf{R}_x^{-1} \mathbf{R}_x^{-T}, \quad (11)$$

where \mathbf{R}_Δ and \mathbf{R}_x are upper triangular square root information matrices. The normalized data, noise and parameter vectors are defined as

$$\mathbf{y} = \mathbf{R}_\Delta \Delta_L, \delta = \mathbf{R}_\Delta \Delta, \mathbf{z} = \mathbf{R}_x \Delta_x, \quad (12)$$

so that the covariance matrices $\Sigma_\delta = \Sigma_z = \mathbf{I}$. After multiplying (10) by \mathbf{R}_Δ , and using $\Delta_x = \mathbf{R}_x^{-1} \mathbf{z}$, the new observation equation in terms of the normalized vectors becomes

$$\mathbf{y} = \mathbf{B}\mathbf{z} + \delta, \quad (13)$$

where $\mathbf{B} = \mathbf{R}_\Delta \mathbf{H} \mathbf{R}_x^{-1}$. Next, the singular value decomposition of the new observation matrix is computed as

$$\mathbf{B} = \mathbf{U}\mathbf{\Lambda}\mathbf{V}, \quad (14)$$

where \mathbf{U} and \mathbf{V} are $l \times l$ and $k \times k$ orthogonal matrices, and

$$\mathbf{\Lambda} = \begin{pmatrix} \Lambda_k \\ \mathbf{0} \end{pmatrix}. \quad (15)$$

Λ_k is a $k \times k$ diagonal matrix containing the singular values λ_i in descending order. Multiplying (13) by \mathbf{U}^T and defining the new data and parameter as $\alpha = \mathbf{U}^T \mathbf{y}$ and $\Phi = \mathbf{V}\mathbf{z}$, we obtain

$$\alpha = \mathbf{\Lambda}\Phi + \Psi, \quad (16)$$

where $\Psi = \mathbf{U}^T \delta$, and $\Sigma_\Phi = \Sigma_\Psi = \mathbf{I}$. The new parameter vector is then separated into two groups by a cutoff singular value $\lambda_c = 1$ so that

$$\Lambda_k = \begin{pmatrix} \Lambda_1 & \mathbf{0} \\ \mathbf{0} & \Lambda_2 \end{pmatrix}. \quad (17)$$

Λ_1 contains all singular values greater than λ_c ; and Λ_2 contains all singular values less or equal to λ_c .

[27] For the new vector observation (16), the LSE without the a priori information would take the form

$$\hat{\Phi}_{\text{LSE}} = \Lambda_k^{-1} \alpha_k, \quad (18)$$

where α_k is a $k \times 1$ vector containing the first k th elements of α . The problem of this estimator becomes apparent when its covariance matrix $\Sigma_{\text{LSE}} = \Lambda_k^{-2}$ is examined. The small singular values in Λ cause large and in many cases unacceptable uncertainties in the estimates even when the inverses of null singular values are all taken to be 0. The best linear estimator (BLE) becomes

$$\hat{\Phi}_{\text{BLE}} = (\Lambda_k^2 + \mathbf{I})^{-1} \Lambda_k \alpha_k. \quad (19)$$

This is also equivalent to LSE with zero a priori mean and the a priori covariance matrix Σ_x . To regularize the small singular values with the a priori information and to reduce the dependence of the estimator on the a priori information which is often unreliable, a hybrid estimator referred as SVD/LSE/BLE hereafter is used throughout this study:

$$\hat{\Phi} = \Gamma \alpha = \begin{pmatrix} \Lambda_1^{-1} & \mathbf{0} & \mathbf{0} \\ \mathbf{0} & (\Lambda_2^2 + \mathbf{I})^{-1} \Lambda_2 & \mathbf{0} \end{pmatrix} \alpha. \quad (20)$$

One can see from the above discussion that $\hat{\Phi}_1$ is the LSE, and $\hat{\Phi}_2$ corresponds to the BLE. The mean square error (MSE) matrix of the estimate is

$$\Sigma_{\hat{\Phi}} = \mathbf{E} \left[(\hat{\Phi} - \Phi)(\hat{\Phi} - \Phi)^T \right] = \Gamma \Gamma^T + (\Gamma \mathbf{\Lambda} - \mathbf{I})(\Gamma \mathbf{\Lambda} - \mathbf{I})^T, \quad (21)$$

where \mathbf{E} is the symbol for mathematical mean, $\mathbf{\Lambda}$ and Γ are the transformed measurement and inverse matrices defined in (14) and (20), respectively. After transforming back to the original parameter space, the estimate becomes

$$\hat{\mathbf{X}} = \mathbf{X}_0 + \mathbf{R}_x^{-1} \mathbf{V}^T \Gamma \mathbf{U}^T \mathbf{R}_\Delta (\mathbf{L} - \mathbf{H}\mathbf{X}_0). \quad (22)$$

The MSE is of the form

$$\Sigma_{\hat{\mathbf{x}}} = \mathbf{R}_x^{-1} \mathbf{V}^T \Sigma_{\hat{\Phi}} \mathbf{V} \mathbf{R}_x^{-T}. \quad (23)$$

For simplicity, the square roots of the diagonal elements of MSE will also be called inversion uncertainties hereafter.

[28] Although the LSE solutions for parameters corresponding to the large singular values do not depend on the a priori model, the parameter transformation and thus the cutoff threshold λ_c which reflects relative a priori accuracy compared with that of data do depend on the a priori covariance matrix. Encouragingly, comparing the RMS degree amplitudes of GRACE data with those of the a priori model shown in Figure 1 indicates that the model predictions are at the right orders of magnitude especially at the lower degrees where GRACE has the most strength. Nevertheless, it should also be noted that many other methods have been proposed more recently with various

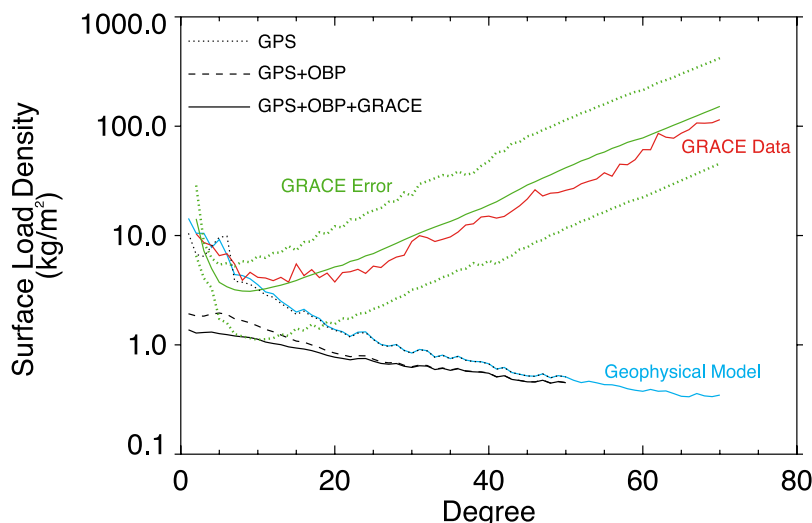


Figure 1. RMS of mean degree amplitudes σ_n (equation (9)) for incremental surface mass density coefficients observed by GRACE (red line) and predicted by a global geophysical model (blue line). The solid green line shows the incremental monthly RMS uncertainty in GRACE-derived density coefficients for each spherical harmonic degree during 2002. The monthly uncertainties have decreased slightly in subsequent years. The dotted green lines indicate minimum and maximum GRACE uncertainties for the $2n + 1$ coefficients within each degree n during a typical month in 2002. The black lines show monthly RMS degree uncertainties (square root of MSE in (23)) resulting from inversions of various data combinations with reduced aid of a priori degree amplitudes (blue line).

assumptions and smoothness criteria about the unknown parameters in this active research field.

[29] To further reduce the amount of a priori information used in the inversion, the a priori covariances of the lowest degrees (1–6 for the case of GPS/OBP) are significantly enlarged so that the longest wavelength surface mass variations are effectively constrained not by the a priori model but by the data. This choice reflects the fact that the geophysical model predicts the largest variations in this degree range (Figure 1). Our previous experience also indicates that the data coverage provides sufficient accuracy for the parameters in this range.

[30] In the case of GPS/OBP/GRACE inversion, it would appear that no a priori information is needed since GRACE data contain spherical harmonic coefficients up to degree and order 70. However, as shown in Figure 1, GRACE gravity based surface mass density has a very unique error spectrum in the spherical harmonic domain. Its uncertainties beyond $n = 10$ grow monotonically and sharply with n , while geophysical model predicted degree amplitudes decay with degree beyond $n = 5$. These indicate that the space gravity measurements are less sensitive to surface mass variations with short spatial scales. The ground based GPS measurements and OBP model, on the other hand, are significantly affected by local small-scale load changes. If the two data sets are simply combined without a priori, the large high-degree GRACE uncertainties will greatly mask the contribution of in situ data to the estimates in the spherical harmonic domain. Other than the low-degree (e.g., $2 \leq n \leq 10$) estimates, which derive most of their information from GRACE data, the results would be analogous to the LSE using GPS/OBP data alone, with very large uncertainties in the spherical harmonic coefficients including those of $n = 1$. Therefore similar to the GPS/OBP

inversion, a priori degree variances need to be used to filter out the increasing noise in the high degree coefficients. Judging from Figure 1, GRACE-derived coefficients from degree 2 to 10 have errors that are generally smaller than the model amplitude. Therefore, in the same spirit of reducing a priori model dependence, we also decide to significantly enlarge the a priori variances for the degree range $1 \leq n \leq 10$ in this case.

[31] Similar to the GPS/OBP inversion, the GPS/OBP/GRACE combination strategy still has a (reduced) dependence on the a priori model and is subject to contamination from its deficiencies. An alternative strategy is to use the degree-1 and zonal degree-2 terms from the combined GPS/OBP/GRACE solution and all other surface mass spherical harmonic coefficients derived from GRACE data alone to form a supplemented GRACE solution.

4. Inversion Results

4.1. Seasonal Surface Mass Variations From GPS/OBP and GRACE Data

[32] To compare with the GRACE results, the detrended and incremental (against March 2004) quasi-monthly GPS data from 446 selected sites and gridded pseudo OBP data are inverted for incremental surface mass density coefficients. The results are first compared with the GRACE-derived surface mass density in the spherical harmonic domain. For seasonal variations, a six-parameter least squares (LS) fit is performed on each GPS/OBP or GRACE-derived coefficient time series of 18 quasi-months according to

$$y(t_i) = a + bt_i + A^a \cos \omega(t_i - \phi^a) + A^{sa} \cos 2\omega(t_i - \phi^{sa}), \quad (24)$$

where ω is the annual angular frequency, t_i is time past 1 January 2000, A^a , ϕ^a , A^{sa} , and ϕ^{sa} are annual amplitude, phase, semiannual amplitude and phase, respectively. Since the linear trends of GPS/OBP data are estimated and removed from longer time series than the 18 GRACE quasi-months, the posteriori linear trends in GPS/OBP-derived surface density coefficients are generally nonzero. These linear trends have little geophysical significance and are removed from the results and discussions. Further, to concentrate on climate-related changes, the oceanic pole tides are also removed from both GPS/OBP- and GRACE-derived surface densities. However, unless noted otherwise, atmospheric contributions are retained in the results.

[33] Figure 2 shows the inverted degree-1 surface mass coefficients based on GPS/OBP data and the GPS/OBP/GRACE data combination. Although GRACE data do not yield estimates for degree-1 coefficients, their strengths over intermediate degree ranges and over the polar areas contribute indirectly to the combined degree-1 estimates. In other words, since GPS/OBP data are sensitive to lump sums of spherical harmonic coefficients of different degrees and cannot resolve them independently (with diagonal posteriori covariance matrix), information about the intermediate degrees coefficients can enhance the power of GPS/OBP data to separate the degree-1 coefficients from these coefficients. This is reflected by smaller error bars for the combination solution. The combined estimate series also provide a better fit to the seasonal variation model. Figure 3 compares 4 degree-2 coefficients derived from GPS/OBP data and from GRACE gravity data. Here, the uncertainties of GPS/OBP results are significantly smaller than those of GRACE results. Overall, the temporal patterns are remarkably similar. The agreements between the relevant pairs of series indicate that the calibrated uncertainties for the GRACE zonal degree-2 estimates are too pessimistic except for the month of January 2004 with only 13 days of data. Figure 4 compares the four low-degree zonal coefficients derived from GPS/OBP and from GRACE. Again, the temporal patterns of the relevant pairs of series are very similar except those for M_{40c} , where the amplitudes are smaller and the series do not really diverge beyond the margin of errors. The fitted annual and semiannual amplitudes and phases for equivalent geocenter motion and low-degree zonal gravity coefficients based on the GPS/OBP and GRACE data are listed in Tables 1 and 2 along with corresponding SLR results. The agreements are striking considering that the two data sets are completely independent and involve such distinctly different measurements.

[34] To further assess and compare the relative strengths of the different data sets and their contribution to the combination, the RMS degree uncertainties resulting from various data sets and combinations are also shown in Figure 1. SVD/LSE/BLE and a priori spectral information ($6 < n \leq 50$ for GPS, GPS+OBP; $10 < n \leq 50$ for GPS + OBP + GRACE) are used for all inversions. Here, the power of data combination is clearly demonstrated including the apparent benefit of adding OBP data to the GPS inversion. Although most of degree uncertainties from data inversions are significantly smaller than those of GRACE, the significant role of the a priori model in the inversions, especially for the high degrees, should be noted.

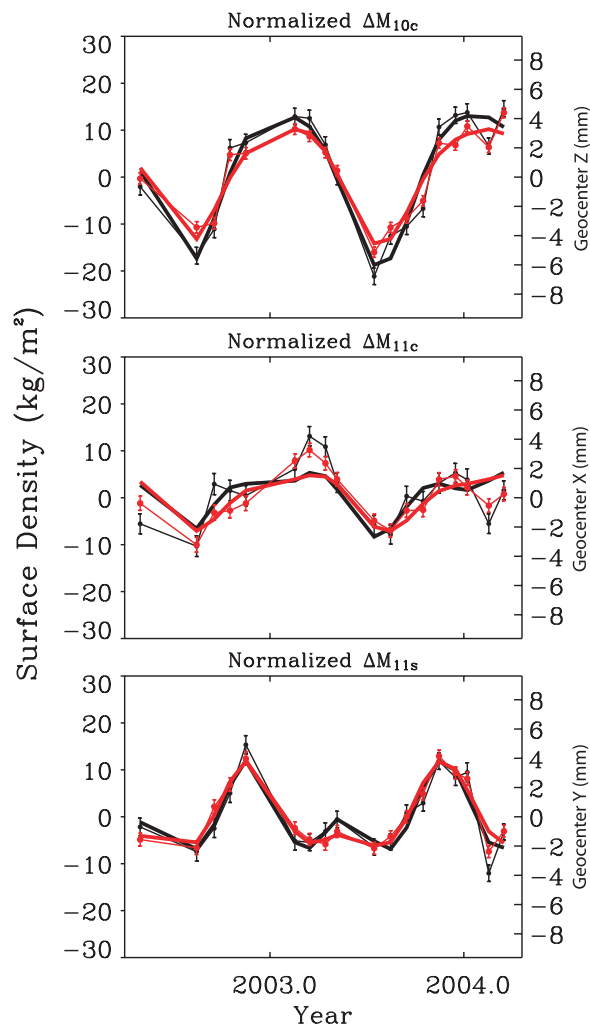


Figure 2. Degree-1 surface mass density coefficients (equivalent geocenter motion on the right scale) estimated from GPS/OBP data (black dots) and from GPS/OBP/GRACE data (red dots). The error bars represent $\pm 1\sigma$ uncertainties. The thick curves indicate six-parameter LS fits to the estimates. Constant biases and linear trends have been removed.

[35] For comparison in the geographic domain and to study seasonal geographic surface mass variations, we fit all spherical harmonic coefficient series ($1 \leq n \leq 50$) estimated from both GPS/OBP and GRACE data with six-parameter models (equation (24)) using their respective full and diagonal covariance matrices. The seasonal coefficients are then mapped to the geographic domain after applying a Gaussian spatial filter [e.g., Wahr et al., 1998] with a half wavelength of 800 km. The covariance matrices are also propagated correspondingly in the fitting, filtering and mapping processes. To remove discrepancies due to the missing degree-1 terms and noisy ΔM_{20c} series in the GRACE data, the same GPS/OBP/GRACE inverted degree-1 and ΔM_{20c} terms are used to replace those in the GPS/OBP results and to supplement the GRACE results. Figure 5 shows and compares the resulting GPS/OBP and GRACE based annual cosine and sine term amplitudes geographically. Their uncertainties are shown in Figure 6.

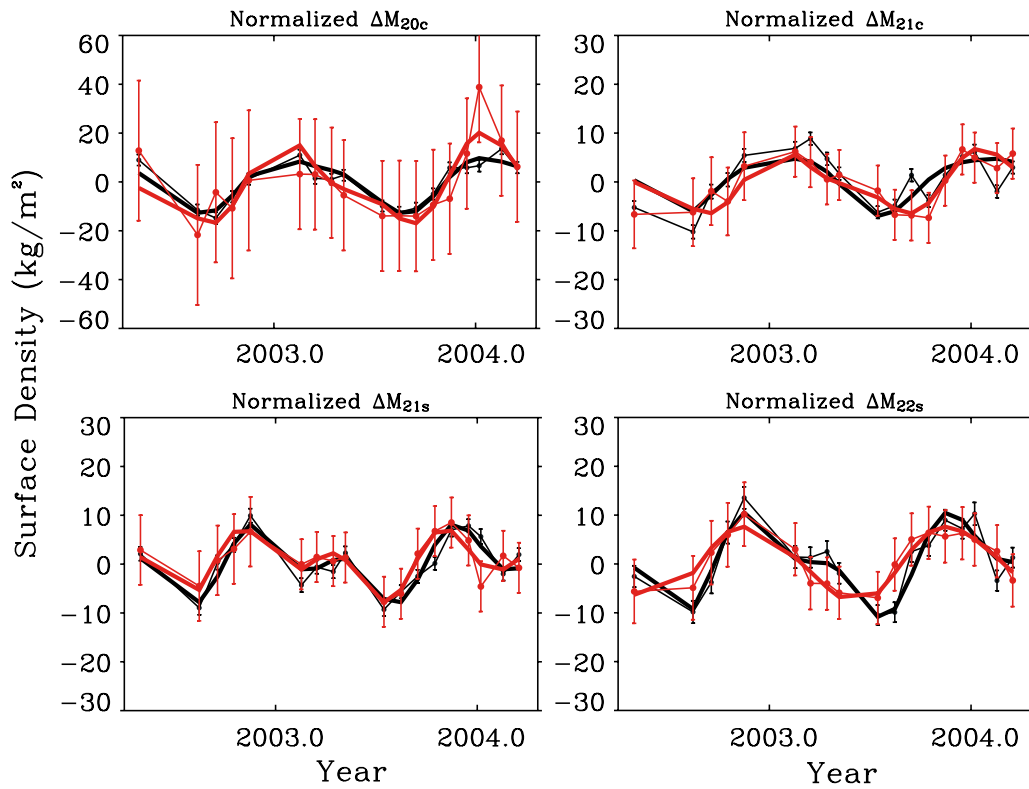


Figure 3. Degree-2 surface mass density coefficients estimated from GPS/OBP data (black dots) and from GRACE data (red dots). Otherwise similar to Figure 2.

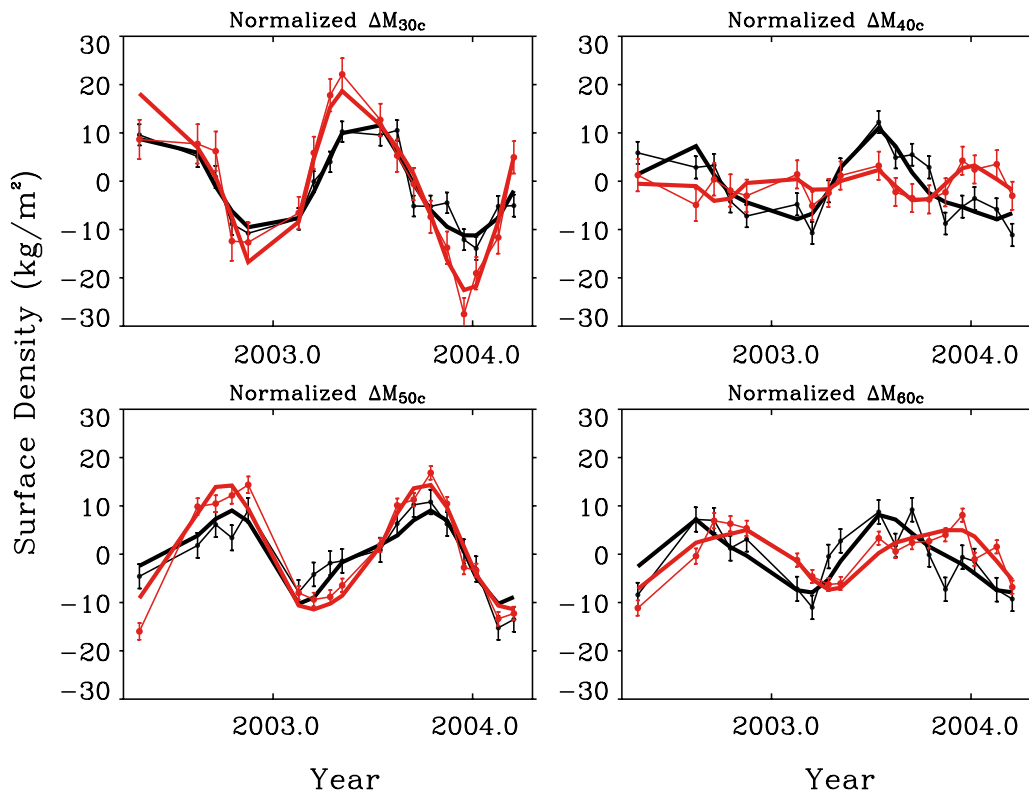


Figure 4. Low-degree zonal surface mass density coefficients estimated from GPS/OBP data (black dots) and from GRACE data (red dots). Otherwise similar to Figure 2.

Table 1. GPS/OBP and GRACE Estimated Annual Surface Mass Variations^a

Δ	A^a				ϕ^a			
	GRACE-18mo	GPS/OBP-18mo	GPS/OBP-5yr	SLR	GRACE-18mo	GPS/OBP-18mo	GPS/OBP-5yr	SLR
X_g	1.8 ± 0.4^b	1.6 ± 0.7	1.7 ± 0.3	2.1 ± 0.5^c	46 ± 15^a	27 ± 21	356 ± 11	48^c
Y_g	2.5 ± 0.3^b	1.9 ± 0.4	3.8 ± 0.3	2.0 ± 0.5^c	329 ± 5^a	326 ± 11	345 ± 4	327^c
Z_g	3.9 ± 0.4^b	5.2 ± 0.5	4.5 ± 0.3	3.5 ± 1.5^c	28 ± 5^a	23 ± 5	21 ± 4	43^c
J_2^d	4.1 ± 0.9	2.8 ± 0.3	2.5 ± 0.2	$2.8, 3.2^e$	215 ± 13	228 ± 8	239 ± 4	$223, 246^c$
J_3	5.0 ± 0.5	3.2 ± 0.4	2.4 ± 0.3	$5.7, 2.0^c$	344 ± 4	352 ± 4	341 ± 7	$19, 6^c$
J_4	0.3 ± 0.2	2.2 ± 0.4	2.1 ± 0.2	$3.2, 1.3^c$	268 ± 57	12.5 ± 8	5 ± 6	$22, 26^c$
J_5	3.0 ± 0.2	1.8 ± 0.3	1.3 ± 0.2	3.7	88 ± 7	73 ± 11	79 ± 8	211
J_6	1.3 ± 0.2	1.6 ± 0.3	1.6 ± 0.2	0.9	119 ± 11	42 ± 13	52 ± 8	23

^aAnnual amplitudes A^a of geocenter components X_g , Y_g , and Z_g are in units of mm. The unnormalized zonal gravity coefficients J_n are in units of 10^{-10} . The ϕ^a are peak times (in days) measured from 1 January.

^bThe geocenter components listed under GRACE-18 mo are the results of the combined GPS/OBP/GRACE solution.

^cFrom *Bouille et al.* [2000].

^dAll SLR zonal J_n except those otherwise noted are from *Cheng and Tapley* [1999]. Their results were wrongly quoted by *Wu et al.* [2003] due to a normalization error on our part and are corrected in this table.

^eFrom *Cox and Chao* [2002].

[36] Overall, the global spatial patterns of the two independent (except 4 common coefficients) results agree quite well. The effects of the $n = 1$ and M_{20c} terms can be isolated by comparing the supplemented and original GRACE solutions (not shown). The most significant geographic features of the supplementation are in the cosine amplitudes with about 2.4 cm reduction at the South Pole and noticeable increase over a large area in Eurasia. The GPS/OBP results over South America and Africa obviously have reduced spatial resolution due to sparse distribution of GPS sites. Nevertheless, similar continent-wide patterns can be seen there in the two estimates for both cosine and sine amplitudes. On the other hand, the cosine amplitudes derived from GPS/OBP are larger than those derived from GRACE over certain areas of North America and Eurasia. The differences, especially those over North America, are apparently statistically significant when the uncertainties in Figure 6 are considered. The cause of these differences is currently unclear. Curiously, the largest difference in the cosine map centers around the junction of Missouri and Mississippi rivers. Unlike the satellite gravity data which measure large area averages, the ground GPS data are more sensitive to local phenomena. It is possible that concentrated local mass variations neither reflected in the a priori model nor accurately recovered by the inversion, errors in GPS measurement models, or seasonally amplified environmental effects [*Ray et al.*, 2005], may have aliased into the GPS/

OBP solutions. It is also possible that the elastic parameters over certain regions may be different from those of the spherical symmetric model used.

4.2. Seasonal Surface Mass Variations Over the Oceans, Antarctica, and Greenland

[37] The incremental mean surface mass in thickness of water equivalent over any particular area can be derived by using (1) and the orthonormal property of the spherical harmonic functions, as

$$\begin{aligned} \Delta h_{mean}(t) &= \frac{1}{\rho_w S_A} \int \int \Delta M(\theta, \phi, t) A(\theta, \phi) \sin \theta d\theta d\phi \\ &= \frac{1}{\rho_w A_{00c}} \sum_{nmq} \Delta M_{nmq}(t) A_{nmq}, \end{aligned} \quad (25)$$

where S_A is the area, $A(\theta, \phi)$ is the area mask function with a value of 1 inside and 0 outside. A_{nmq} is the spherical harmonic coefficient of A . Equation (25) is then applied to the global oceans, Antarctica, and Greenland using our combined GPS/OBP/GRACE and supplemented GRACE solutions of total surface mass (including ocean and atmosphere) coefficients ΔM_{nmq} . The supplemented GRACE solution here uses the degree-1 and zonal degree-2 coefficients estimated from GPS/OBP/GRACE data combination. Mean surface mass variations after removing

Table 2. GPS/OBP and GRACE Estimated Semiannual Surface Mass Variations^a

Δ	A^{sa}				ϕ^{sa}			
	GRACE-18mo	GPS/OBP-18mo	GPS/OBP-5yr	SLR	GRACE-18mo	GPS/OBP-18mo	GPS/OBP-5yr	SLR
X_g	0.6 ± 0.4^b	1.0 ± 0.7	1.0 ± 0.3	1.1^c	121 ± 23^b	104 ± 17	118 ± 9	145^c
Y_g	1.3 ± 0.2^b	2.0 ± 0.4	0.9 ± 0.3	0.8^c	143 ± 5^b	144 ± 6	143 ± 10	120^c
Z_g	0.8 ± 0.4^b	1.0 ± 0.5	0.6 ± 0.3	0.4^c	110 ± 14^b	115 ± 15	113 ± 15	39^c
J_2^d	1.6 ± 1.0	0.8 ± 0.4	0.6 ± 0.2	1.2	92 ± 15	67 ± 13	83 ± 10	72
J_3	1.2 ± 0.4	0.4 ± 0.3	0.3 ± 0.3	2.5	7 ± 9	66 ± 23	136 ± 29	40
J_4	0.8 ± 0.2	0.7 ± 0.4	0.5 ± 0.2	1.1	88 ± 7	87 ± 14	83 ± 11	148
J_5	0.5 ± 0.3	0.7 ± 0.3	0.2 ± 0.2	2.3	13 ± 17	38 ± 13	49 ± 25	148
J_6	0.3 ± 0.2	0.4 ± 0.4	0.2 ± 0.2	0.7	102 ± 18	89 ± 20	53 ± 34	93

^aThe units and conventions of semiannual amplitudes A^{sa} and peak times ϕ^{sa} are similar to those in Table 1.

^bThe geocenter components listed under GRACE-18 mo are the results of the combined GPS/OBP/GRACE solution.

^cFrom *Eanes et al.* [1997].

^dAll SLR zonal J_n are from *Cheng and Tapley* [1999]. The mistakenly quoted results in *Wu et al.* [2003] are also corrected here.

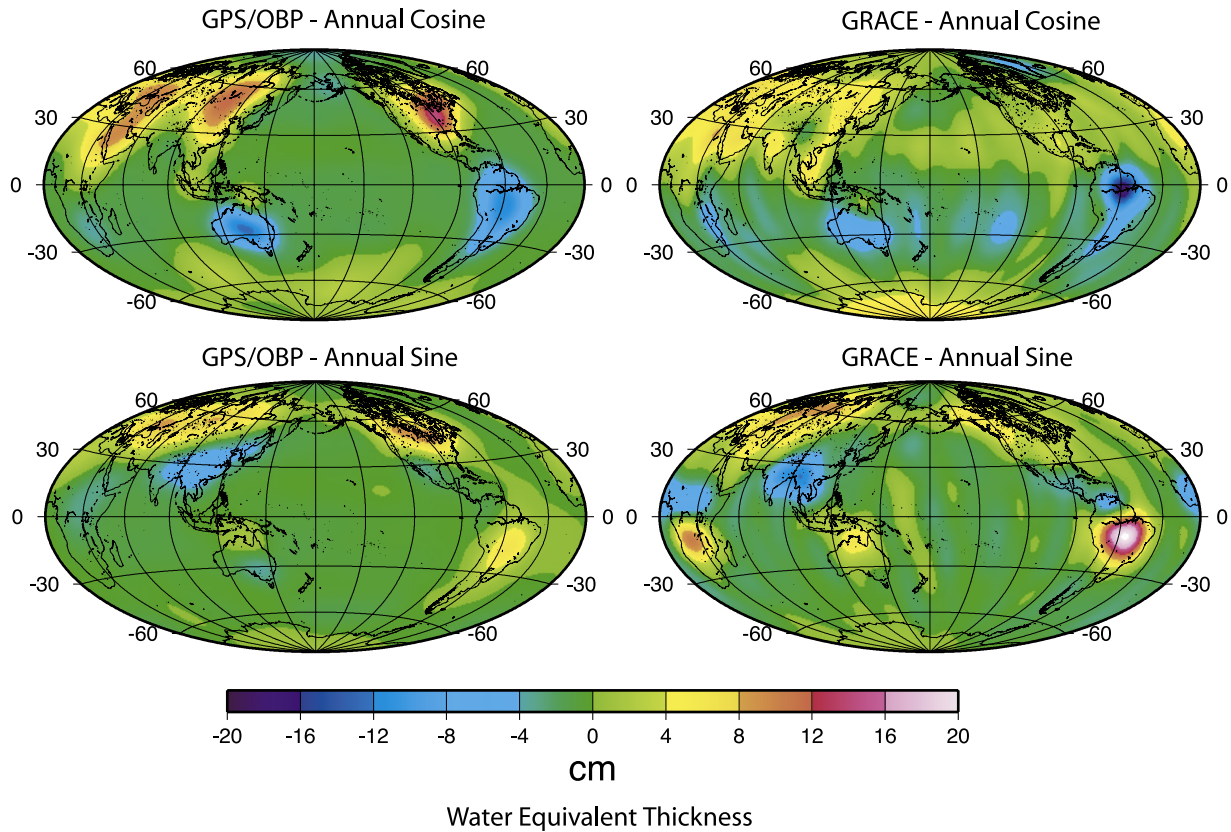


Figure 5. Annual in- and out-of-phase surface mass variation (including the atmosphere) amplitudes derived from GPS/OBP and from GRACE after a Gaussian filter with half wavelength at 800 km is applied to both; $t = 0$ at 1 January. The same degree-1 and zonal degree-2 coefficients derived from GPS/OBP/GRACE inversion are also used to replace those in the GPS/OBP results and to supplement the GRACE results.

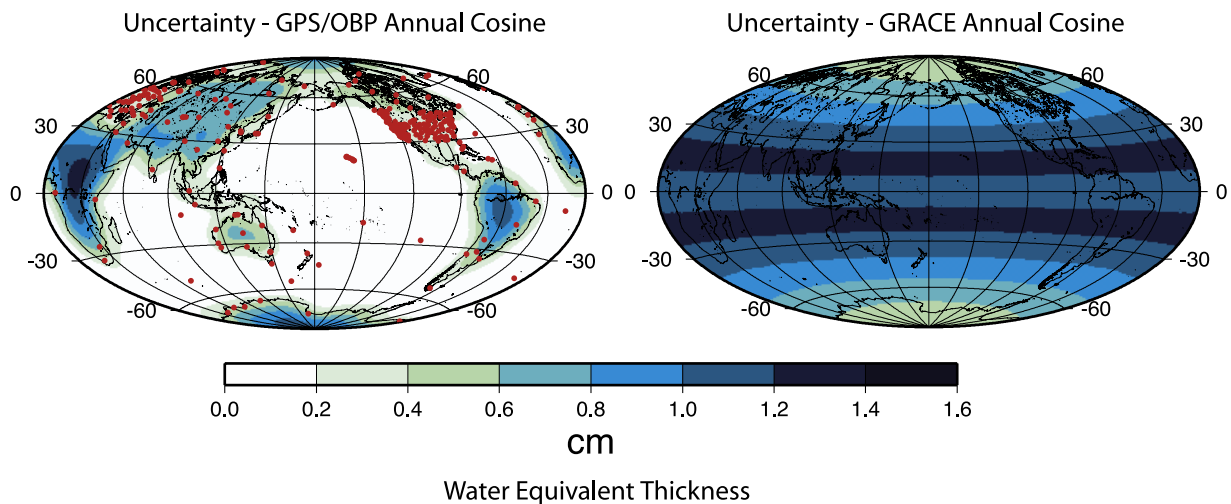


Figure 6. Uncertainties in annual in-phase surface mass variation amplitudes derived from GPS/OBP and from supplemented GRACE coefficients after applying the 800-km Gaussian filter. The out-of-phase amplitude uncertainties are slightly smaller and are not shown. The red dots indicate locations of 446 continuous GPS sites used in the study.

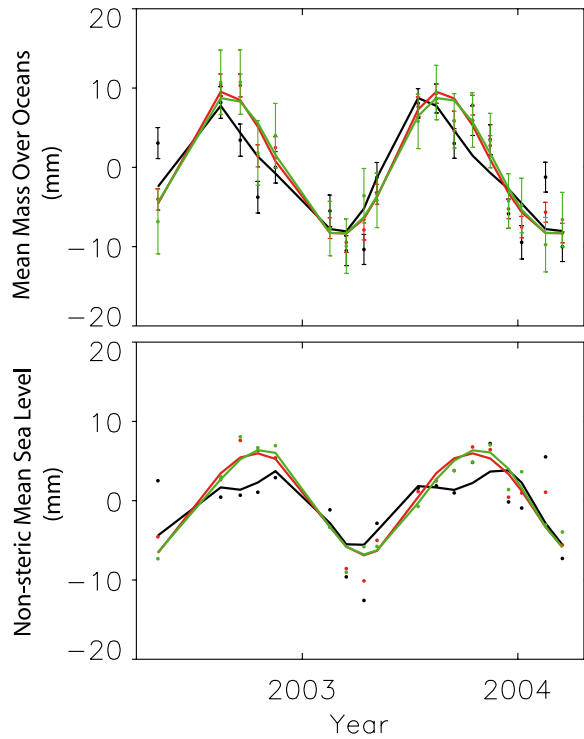


Figure 7. (top) Total incremental surface mass averaged over the global oceanic area in thickness of water equivalent derived from GPS/OBP (black), GPS/OBP/GRACE data (red), and supplemented GRACE solution (green). Dots are quasi-monthly estimates, and error bars represent $\pm 1\sigma$ uncertainties. Thick curves show six-parameter LS fits to the estimates. Constant biases and linear trends are removed from both estimates and fitted models. (bottom) Similar to Figure 7 (top), except it is for incremental average oceanic mass after removing the average atmospheric mass over the oceans.

the atmosphere are also computed for these areas (with $\Delta M_{00c}(t)$ retained).

[38] Our spherical harmonic coefficients are truncated at degree 50 to 70 due to computing and data limitations. To derive area means, we experimented with the supplemented GRACE coefficients using truncation degrees of 50 and 70, and Gaussian filters with half wavelengths ranging from 0 to 400 km. For the large area average over the global oceans, no significant differences beyond statistical uncertainties are found among these different solutions except the case of degree-70 truncation with insufficient filtering. For

example, the unfiltered harmonic series in (25) up to degree 50 and the 400-km Gaussian-filtered harmonic series up to degree 70 yield essentially the same annual total mass variation over the oceanic area. For Greenland and Antarctica, at the truncation degree of 50, the mean amplitudes decrease with increasing filter wavelength. However, the reduction in the uncertainties are fairly moderate. Therefore we adopt a simple averaging approach of truncating the harmonic series at degree 50 without filtering. Such a spatial averaging kernel is very similar to the mask function when the truncated higher-degree terms are assumed to be small.

[39] Figure 7 (top) shows the mean mass over the global oceanic area in thickness of water equivalent derived from the GPS/OBP solution, combined GPS/OBP/GRACE solution and supplemented GRACE solution, respectively. All three solutions exhibit similar temporal patterns with excellent agreements among the annual amplitudes and phases within their respective uncertainties (Table 3). To derive the mean oceanic mass, or equivalently, the non-steric mean sea level, we compute the mean atmospheric mass over the global oceans using NCEP reanalysis surface pressure fields and remove them from the total mass over the oceans. The averaging is carried out over the 2.5×2.5 global oceanic grid with a $\sin \theta$ cell weighting. All mixed land/ocean cells are regarded as land cells and removed from the calculation. The resulting mean oceanic mass from the three solutions are shown in Figure 7 (bottom) and in Table 3. Compared with the GRACE related solutions, the GPS/OBP solution underestimates the annual amplitude by more than 2 mm. This is not inconsistent with its largest amplitude uncertainty among the three solutions. The combined GPS/OBP/GRACE and supplemented GRACE solutions also result in better accuracies and in increasing order, better fit to the seasonal cycles.

[40] Figure 8 shows the mean mass (including the atmosphere) variabilities derived from the combined GPS/OBP/GRACE and supplemented GRACE solutions over Antarctica and Greenland in thickness of water equivalent. Our GPS/OBP solution severely undersamples these areas and will not be discussed further. The annual amplitudes and phases are also listed in Table 3. The mean thickness variations are clearly an order of magnitude larger than that of the oceans. The peak times for both areas seem to fall within their hemispherical summer seasons. This behavior may be a result of increased moisture-holding capacity of the atmosphere with warmer temperatures in the very cold regions of the Earth [Van der Veen, 1991]. This peculiar temporal pattern is largely reversed when the atmospheric contribution is removed

Table 3. Annual Mass Variation Averaged Over the Global Oceans, Antarctica and Greenland in Thickness of Water Equivalent

Solution	Atmosphere+Ocean Mass		Oceanic Mass		Antarctic Mass		Greenland Mass	
	A^a , mm	ϕ^a , days	A^a , mm	ϕ^a , days	A^a , mm	ϕ^a , days	A^a , mm	ϕ^a , days
GPS/OBP	7.7 ± 1.6	222 ± 12	3.9 ± 1.4	285 ± 29				
GPS/OBP/GRACE	9.0 ± 0.7	238 ± 6	6.4 ± 0.7	288 ± 9	40 ± 12	8 ± 13	51 ± 11	182 ± 9
Supplemented GRACE	8.7 ± 0.7	241 ± 6	6.6 ± 0.6	292 ± 7	61 ± 14	11 ± 10	76 ± 14	174 ± 7
Supplemented GRACE-ATM					14 ± 4	204 ± 14	43 ± 7	74 ± 14
Chambers et al. [2004]			8.4 ± 1.1	270 ± 8				

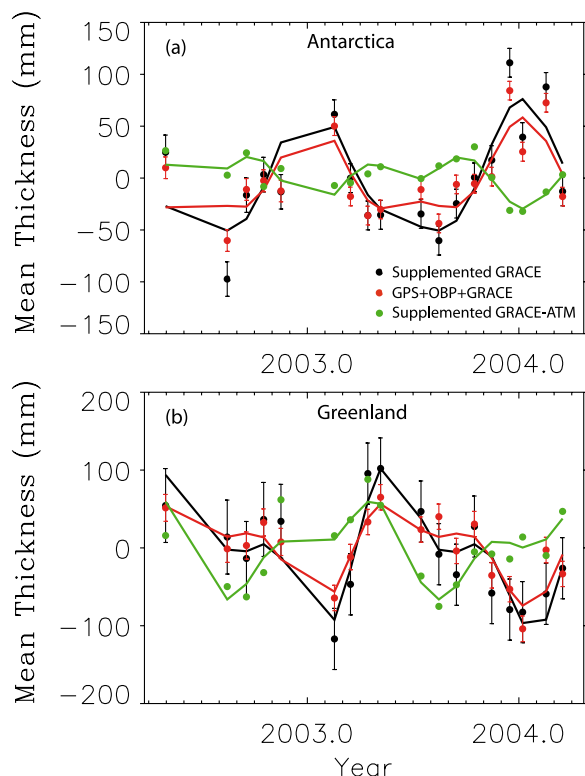


Figure 8. Total incremental surface mass averaged over (a) Antarctica and (b) Greenland in thickness of water equivalent derived from supplemented GRACE data (black) and from GPS/OBP/GRACE combination (red). The green dots and curves are quasi-monthly supplemented GRACE results and LS fit after atmospheric contribution has been removed.

from the estimated total mass. The mean mass on land for both Antarctica and Greenland shows positive balance in their respective winters with smaller amplitudes (Table 3). Figure 9 illustrates the spatial pattern of the fitted annual total mass variations over Antarctica from the 800 km Gaussian-filtered supplemented GRACE solution. The increased mass in summer (Figure 9a) appears to center in the central regions of East Antarctica. Most of the mass variation, however, occurs in the atmosphere with smaller contribution from surface accumulation and ablation (Figures 9c and 9d).

[41] Our supplemented GRACE solution for annual nonsteric sea level variation amplitude differs from that of *Chambers et al.* [2004] by 1.8 mm. Our result includes the concurrent nonatmospheric $n = 0$ and $n = 1$ terms for the GRACE quasi-months. The different supplemental data used, respective uncertainties, and slightly different sampling periods should also be noted. Our nonatmospheric Greenland mean mass variation results (green dots in Figure 8b) compare favorably with those of *Velicogna et al.* [2005] before 2004. Our peak-to-peak variation is also 16 cm water equivalent. However, our results do not show the clear minimum at the beginning of 2004 seen in their results. Our minimums usually occur during late summers which seem to agree better with a surface mass balance model shown by them. Again, although there are systematic differences in the respective results, the statistical uncertain-

ties are quite large at this early stage, which is especially true for our unfiltered mean mass variation with a maximum degree of 50 and a typical quasi-monthly uncertainty of 4 cm.

4.3. Seasonal Surface Mass Variations From 5 Years of GPS/OBP Data

[42] To further investigate the seasonal mass variations, we use GPS data from 457 selected sites with more than 2 years of tracking history, and gridded pseudo OBP data during 1993 to March 2004. The data are cleaned, monthly averaged, detrended, and then differenced against those of March 2004. Following the same inversion procedure and removal of the oceanic pole tides, the results between 1999 and March 2004 are again fitted to (24) using the LS method for seasonal variations. This period has improved GPS coverage and is not impacted by a major El Niño–Southern Oscillation (ENSO) event.

[43] The monthly errors in the data are assumed to be statistically independent while the monthly estimate uncertainties, in fact, include bias terms which may not average down as random noise. This becomes a concern particularly for the long time series. To investigate the possibility of overly optimistic estimates of seasonal uncertainties, we conducted a simultaneous inversion of the GPS/OBP data between 1999 and March 2004. Using the six-parameter model (24) for each spherical harmonic coefficient, all parameters of spherical harmonic coefficients up to degree and order 20 are solved for together. The a priori degree variances are also constructed for the model parameters using the geophysical model. The resulting low-degree seasonal uncertainties, however, are at the same levels as those obtained by the LS fit to monthly inversion results after both are scaled by the a posteriori unit weight uncertainties, respectively. It is possible that part of the systematic errors omitted by the uncertainty estimates in the fits are compensated by irregular surface mass variations contributing to posteriori unit weight uncertainty. Another possibility is that the fit results are not significantly aliased by seasonal variations. With quantitatively similar seasonal estimates, the simultaneous inversion apparently increases our confidence in the seasonal uncertainties.

[44] Figure 10 shows the degree-1 surface mass coefficients with oceanic pole tide and the residual linear trends removed. Clear annual cycles can be seen in all three coefficients. Similar results are also found but not shown here for other low-degree coefficients. The mean annual and semiannual amplitudes and phases of converted geocenter (5) and low-degree zonal gravity coefficients during this period are also listed in Tables 1 and 2. Compared with the 5-year GPS-only inversion results reported by *Wu et al.* [2003], the addition of the pseudo OBP data achieves more than a factor of 3 improvement in the low degree and order coefficients. The annual cycles become much more significant with considerably better fits to the inverted time series. Compared to the GPS/OBP results over the 18 GRACE quasi-months, no significant change is found for the annual cycles over the longer period. The semiannual geocenter motion agrees quite well with that from SLR even though their time windows differ. The semiannual zonal gravity estimates, on the other hand, are considerably smaller than those from SLR. In fact, except the geocenter X and Y results, all semiannual amplitudes found in our study, are

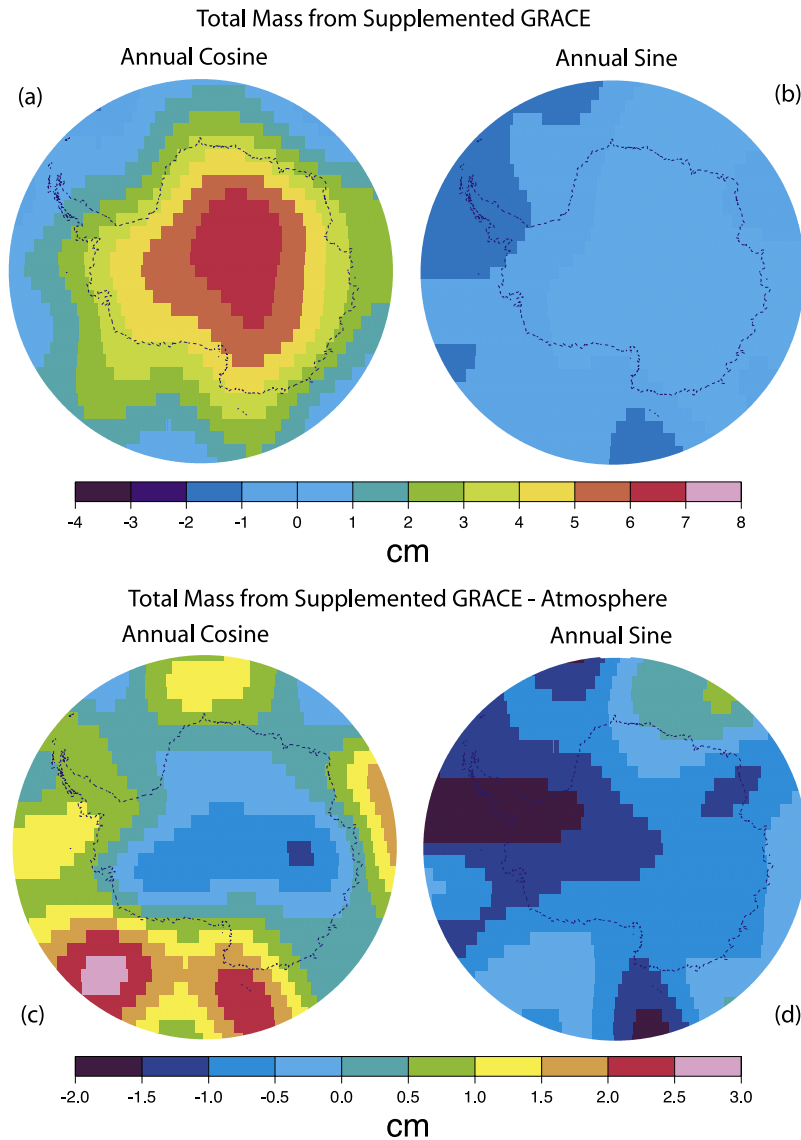


Figure 9. Similar to Figure 5 except it is for annual in-phase and out-of-phase amplitudes over Antarctica derived from supplemented GRACE data. (a) and (b) Annual amplitudes including atmospheric contributions. (c) and (d) Annual amplitudes after atmospheric mass has been removed.

fairly small and not statistically significant when compared with their uncertainties.

[45] The annual mean cosine and sine amplitudes between 1999 and March 2004 are illustrated in Figure 11. Compared with the GPS/OBP results over the 18 GRACE quasi-months in Figure 5, the cosine amplitudes here become much subdued over North America while increase slightly over Asia. The sine amplitudes are similar to the GPS/OBP results in Figure 5 except for even lower amplitudes in South America.

4.4. Interannual Surface Mass Variations From GPS/OBP Data

[46] The GPS/OBP inverted results from 1993 to March 2004 with 457 continuously tracking stations also show significant interannual variations. The atmosphere contributes only slightly at this timescale and is removed along

with oceanic pole tide from the total incremental surface mass. Figure 12 shows three low-degree zonal incremental surface mass change in equivalent geocenter motion and gravity coefficients. The thick curves and the parallel thin curves indicate running annual averages and their respective $\pm 3\sigma$ uncertainties. Figure 12 points to extremes near the 1997–1998 ENSO event. The ΔJ_2 and ΔJ_3 results both compare quite favorably with those of *Cox and Chao* [2002], with a J_2 reversal starting in 1998. Moreover, our GPS/OBP results up to 2004 also show a clear downward trend completing in 2002, indicating that the reversal was largely a part of an interannual cycle when compared with the SLR result. However, our results by themselves contain no information on any new permanent or secular trend since the GPS/OBP data have been detrended prior to the inversion. The agreement over the interannual J_2 cycle between SLR and our GPS/OBP inversions also indicates that the

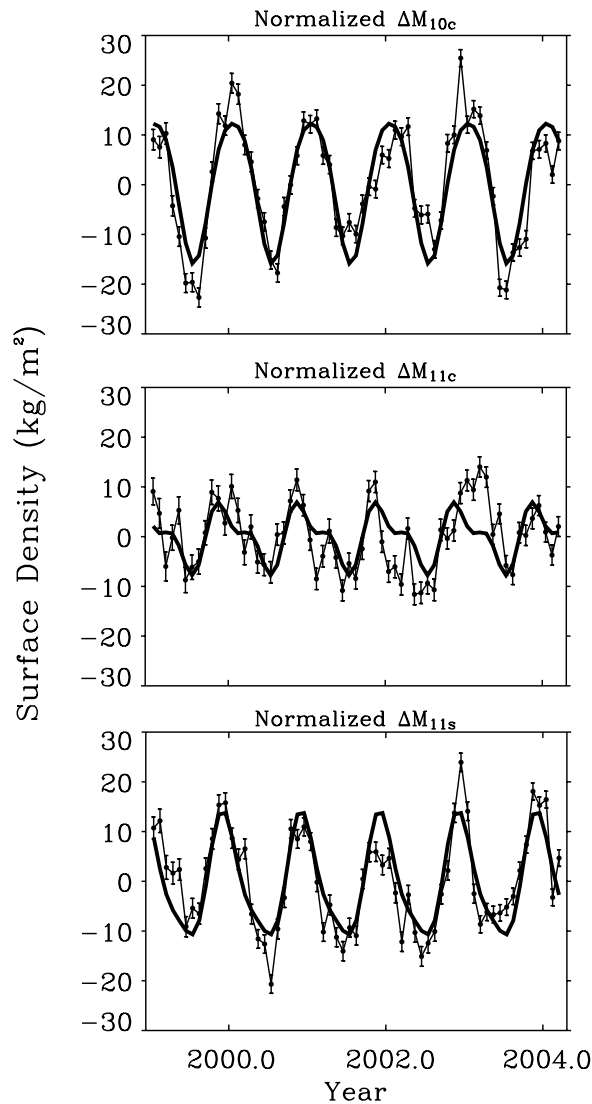


Figure 10. Similar to Figure 2 except it is for GPS/OBP-derived degree-1 coefficients from 1999 to March 2004.

variation is unlikely to be predominantly due to an unmodeled dispersive 18.6-year tide [Benjamin *et al.*, 2003], since the residual tidal signature in the GPS data would result in a very different J_2 variation pattern (with an opposite sign) when inverted as load-induced deformation.

[47] Our GPS/OBP results also contain a full spectrum of the spherical harmonic variations up to degree and order 50. These can be mapped geographically to better identify and understand the sources of change. We first compute annual averages each year for all the inverted spherical harmonic coefficients and then apply a Gaussian spatial filter with a half wavelength of 400 km before mapping. The Gaussian filter is not essential here because the high-degree harmonics are already damped by the a priori information in the inversion. It nevertheless further reduces the geographic errors by factors up to 2. Figure 13 shows successive annual mean differences between 1996, 1998, 2000, and 2002 in thickness of water equivalent. The uncertainties of two representative annual differences can be seen in Figure 14

with GPS site distributions in 1996 and 1998. Very large interannual variations beyond nominal statistical uncertainties can be seen from Figures 13 and 14. From 1996 to 1998, there was a southward mass movement on both Eurasia and North American continents, consistent with the low-degree zonal trends seen in Figure 12. The movement in Eurasia actually started in 1994 with a persistent annual mass shift toward the south. Although it is tantalizing to speculate a decade-long change in permafrost watershed balance [e.g., Yamazaki *et al.*, 2006] associated with ongoing Arctic and sub-Arctic warming [Serreze and Barry, 2005], we should note that the early GPS data coverage (before 1996) in the central Asia area is very sparse. The mass movement reversed direction in years after 1998, again, suggesting that a significant part of the variations (including the 1998 J_2 reversal) may be an interannual cycle. A much wetter Amazon in 2000 and increased mass over Australia and Antarctica in 1998 can also be seen.

[48] The total mean mass over the oceanic area and the mean nonsteric sea level inverted from GPS/OBP data are shown in Figures 15 (top) and 15 (bottom), respectively. Over the 11-year period, Figures 15 (top) and 15 (bottom) show considerable interannual variations. The fitted mean annual cycle in the total average mass closely follows that of the mean atmospheric mass over the oceans with an amplitude of 6 mm and a peak occurring in mid-July. The temporal pattern of the mean oceanic mass over this period is highly structured with large year-to-year variability but no clear mean annual cycle.

5. Discussion and Conclusions

[49] Surface mass variations leave distinct signatures in both time-variable gravity and crustal deformation which are accurately measured by the GRACE mission and global continuous GPS network. The relative oceanic mass distribution is also adequately represented by the data-assimilated OBP model. To validate and complement GRACE data, we conduct global inversions of surface mass variations parameterized in the spherical harmonic domain. Our results yield a complete spectrum of coefficients up to degree and order 50. To achieve meaningful low degree and order coefficients, a priori information has to be used when point GPS measurements are used. We desire solutions of the inverse problem using as little a priori information as possible in order to minimize contamination from poor, or unreliable, information. First, our reduced prior information consists only of degree variances for $n > 6$ or $n > 10$ coefficients from the combined global model of atmosphere, oceans and land hydrology. The a priori spectrum is not significantly inconsistent with that of the GRACE data (Figure 1). Second, we use a hybrid of LSE and BLE estimators under the platform of SVD so that only those components of the a priori information is used when their uncertainties are smaller than those of equivalent data. The hybrid estimator also proves to be effective in cases of heterogeneous data coverage such as the GPS network.

[50] Incorporation of the pseudo-ECCO OBP data into the GPS inversion improves the results dramatically in spite of the Boussinesq approximation and lack of mean mass information. The data-assimilated ocean model accurately represents spatially relative mass variations associated with

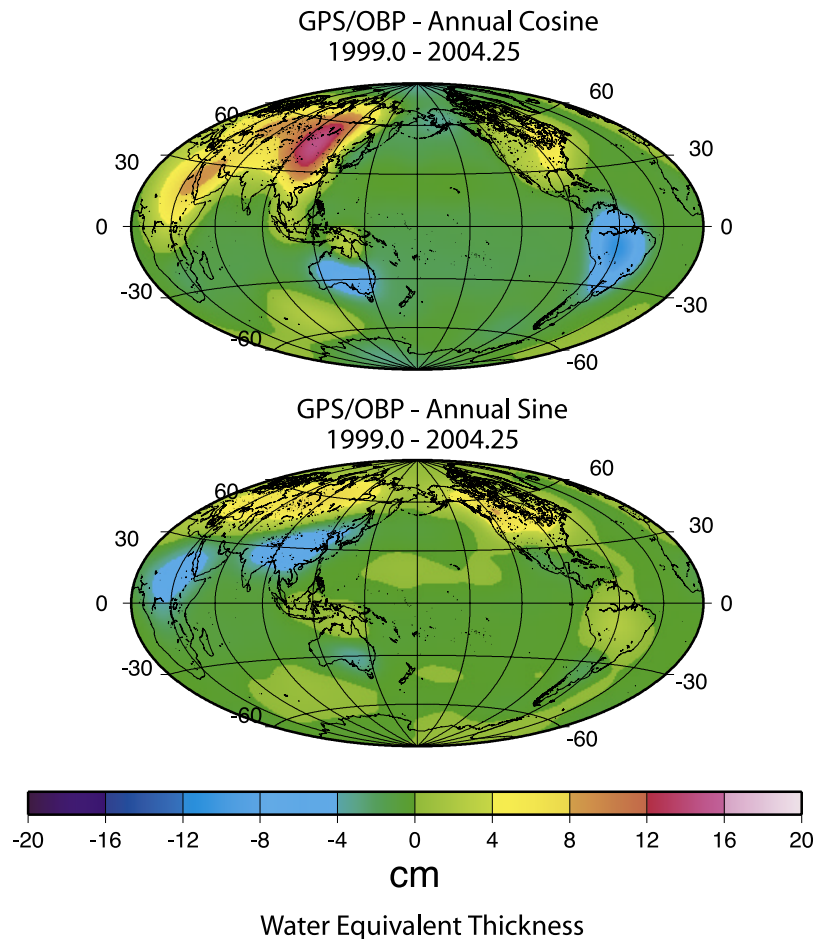


Figure 11. Similar to Figure 5 except it is for annual amplitudes estimated using GPS/OBP data from 1999 to March 2004.

oceanographic phenomena over 2/3 of the surface area of the Earth where GPS data coverage is restricted to a small number of islands. The mean mass over the oceanic area is parameterized as eustatically (uniformly) distributed and estimated from the geodetic data. Currently, time-variable geoid is not featured in the ECCO model and gravitationally self-consistent sea level distribution is not enforced in the inversion. However, some allowance of geographic sea level signature is permitted by the uncertainties in the pseudo OBP data. It is not currently known whether this approximate arrangement is sufficiently accurate or biased so as to contribute to the underestimation of the nonsteric mean sea level from GPS/OBP data. A more rigorous treatment in the future is desirable.

[51] The GPS/OBP inversions yield accurate results for low degree ($n \leq 6$) spherical harmonic coefficients of the incremental surface mass. Some individual higher-degree coefficients are not well recovered due to data coverage gaps on certain continents and polar regions. However, many of linear combinations involving these coefficients are accurately determined. For example, mapping the spherical harmonic series to the densely tracked regions of North America and Eurasia achieve high resolution and accuracy results there.

[52] The GPS/OBP inverted low degree harmonic coefficients and global geographic patterns of surface mass variation agree very well with those of GRACE. These are clear signs of validation of both data types and the important geophysical hypothesis that the dominant source of time-variable gravity and crustal deformation at the seasonal and interannual scales is surface mass variation. However, the GPS measurements are also sensitive to a number of other geophysical and instrument effects. Although we have removed significant seismic deformation and certain known aquifer and oil field related signals from the data, it is likely that this effort is not complete. Also, concentrated local activities unlikely to be reflected in the a priori degree variances and not accurately recovered by the inversion can significantly contaminate the results in the regions. More importantly, instrument and environment effects on radio propagation with possible seasonal correlation may also contaminate the geophysical results. Such errors may explain some of regional differences found in comparison with the GRACE results. However, consistent with the overall agreement with GRACE, the various GPS errors are hopefully isolated in time and space and averaged down on our larger spatiotemporal scales.

[53] The GPS/OBP and GPS/OBP/GRACE combinations both yielded very accurate results on degree-1 and -2

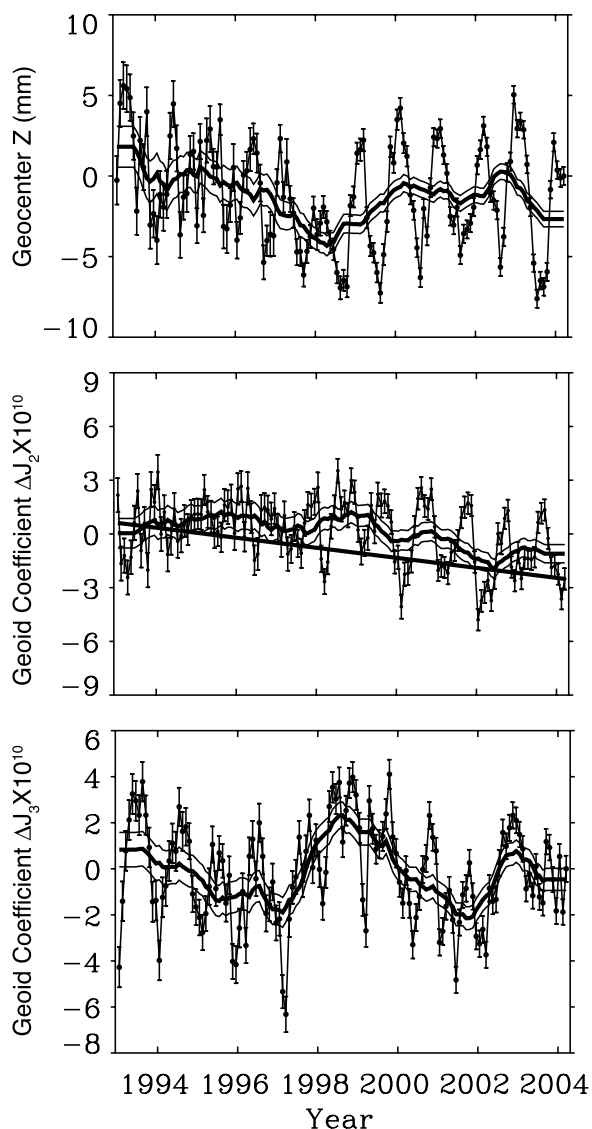


Figure 12. (top) GPS/OBP estimated geocenter motion component Z_g and (middle and bottom) low-degree zonal gravity coefficients. Dots are monthly estimates with error bars indicating $\pm 1\sigma$ uncertainties. Thick lines are annual running averages with two parallel thin lines indicating $\pm 3\sigma$ uncertainties. Atmospheric contributions are removed. Linear trends have been removed from GPS/OBP data before inversion. A linear trend of $-2.8 \times 10^{-11} \text{ yr}^{-1}$ is added to the ΔJ_2 results for comparison with those of *Cox and Chao* [2002].

surface mass coefficients. The GPS/OBP/GRACE degree-1 results correspond to equivalent geocenter motion with annual amplitude precisions better than 0.5 mm in all three components, which is significantly smaller than the likely 1 mm accuracy limit for SLR due to its sparse network. These undoubtedly complement the GRACE data to form a complete spherical harmonic spectrum with significant benefit to the study of ice mass balance in the polar areas, nonsteric sea level change, and polar motion [Gross *et al.*, 2004]. For example, using the GPS/OBP/GRACE com-

bined degree-1 plus zonal degree-2 coefficients with the rest of GRACE data resulted in over 2 cm improvement in the determination of annual mean Antarctic mass balance.

[54] Both the GPS/OBP and GRACE solutions indicate a clear seasonal north/south hemispherical asymmetry in mass distribution over continents in rough accord with solar irradiance and temperature distribution. The polar areas, however, are exceptional to such accord. Our supplemented GRACE solution and GPS/OBP/GRACE combined solution show statistically significant positive mass balances for both Greenland and Antarctica in their respective summers. If we rely on the predictions of the NCEP/NCAR reanalysis surface atmospheric pressure model, this mass variability is due to atmospheric seasonality. The land components of the mass variations, having smaller amplitudes, still roughly follow the above mentioned accord. Obviously, a different mechanism such as temperature-dependent moisture-holding capacity of the atmosphere, may be responsible for the seasonal cycles in the cold regions. Our two GRACE-related solutions yield essentially the same results on the total mass over the oceanic area with submillimeter uncertainties. The GPS/OBP inversion, on the other hand, results in a noisier, but much longer, time series. After removing the total atmospheric mass over the oceans, the resulting 11-year nonsteric sea level series shows pronounced interannual variability and a changing temporal pattern with no clear mean annual cycle. One factor in deriving the nonsteric sea level is the total atmospheric mass above the oceans. Although atmospheric models are generally regarded as more accurate than the other mass components on the Earth's surface, it is possible that the total mass above the oceans may have considerable errors due to undersampling and model deficiencies. Such errors will directly affect our nonsteric sea level estimation. However, it is also possible that the two-way continent-ocean mass transport has interannual variability as noted recently by *Ngo-Duc et al.* [2005].

[55] Our long time series of GPS/OBP solutions also show global interannual surface mass variations with significant amplitudes in the Northern continents and over the Amazon. A dominant feature is the north to south mass movement before 1998 over Eurasia and North America. The movement, however, is largely reversed from 1999 to 2002. Although our mass transport results have been detrended, when combined with the SLR J_2 pattern, both tend to suggest a largely interannual process rather than any newly established long term trend. The interannual variations are significantly beyond statistical uncertainties. However, the data coverage over the vast Eurasian continent was sparse during the earlier years before 1998. The possibility of significant regional aliasing due to instrumental, environmental, and local geophysical effects, and deficiencies in the a priori model cannot be completely ruled out during this time. The validity of the GPS results in this region depends more on the smoothness of mass variation assumed in the a priori model. On the other hand, the mass movement correlated in time with the ENSO events and related global mean surface temperature. Therefore the GPS results, at the least, support the scenario that ENSO related temperature fluctuations can lead to degradation and aggradation of the permafrost and ice in the subarctic regions [e.g., *Demek, 1994*]. More confidence can be placed on the

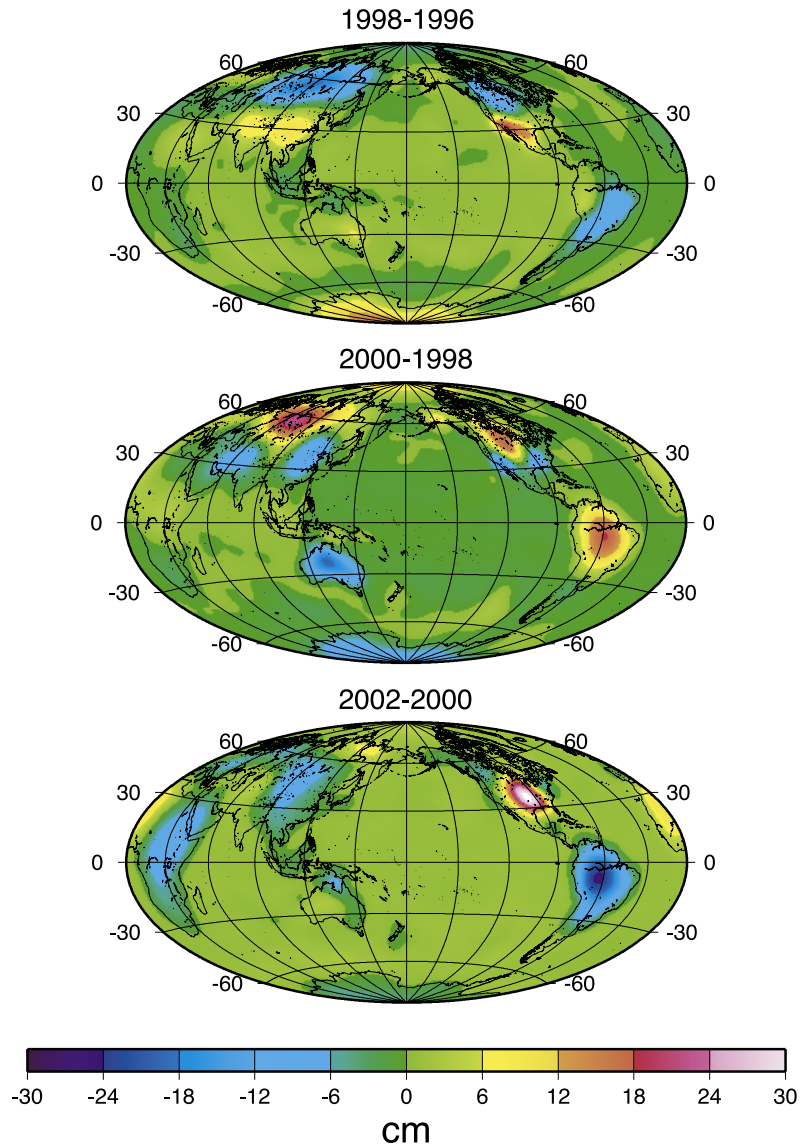


Figure 13. Interannual surface mass variations (excluding the atmosphere) in thickness of water equivalent estimated from GPS/OBP data. Successive differences of annual mean surface mass in thickness of water equivalent are shown.

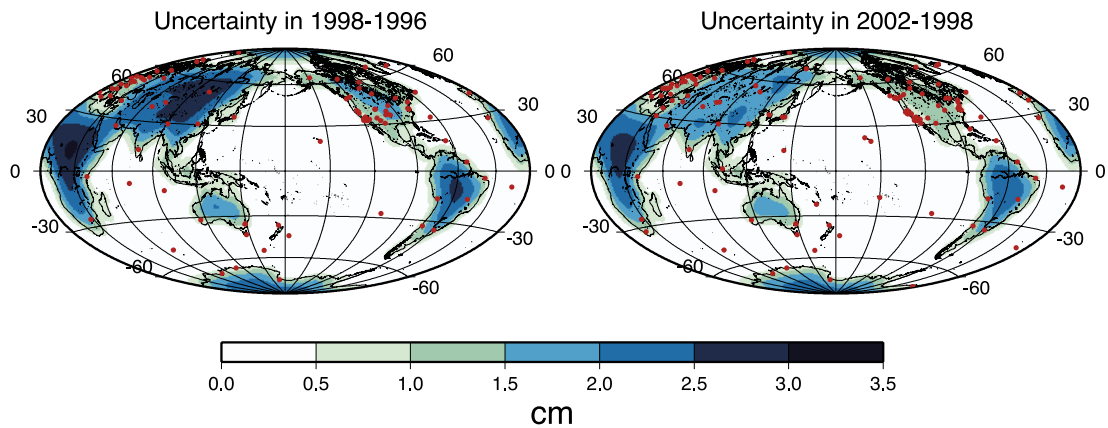


Figure 14. Representative uncertainties in two differences of annual mean surface mass distribution estimated from the GPS/OBP data. Red dots indicate used GPS sites for 1996 (left) and 1998 (right).

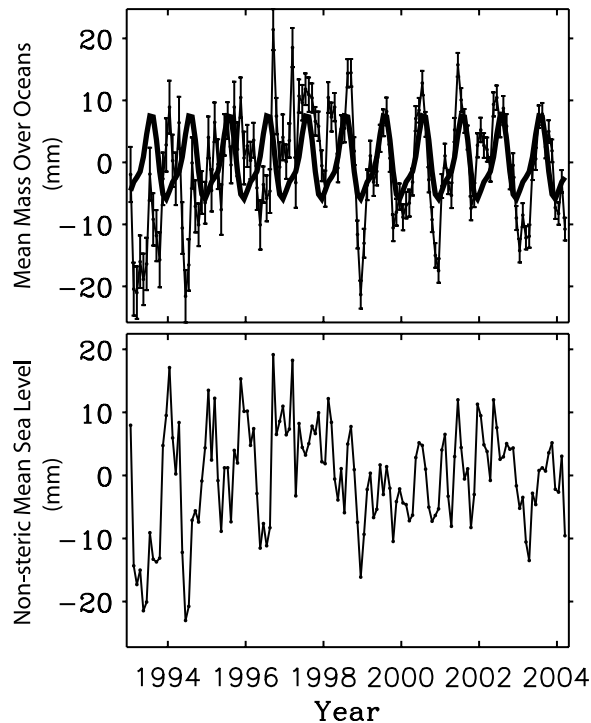


Figure 15. GPS/OBP estimated incremental surface mass averaged over the global oceans from 1993 to March 2004. Otherwise similar to Figure 7.

estimated interannual variations for North America and after 1998. Our solutions also suggest that the primary contributor to the anomalous J_2 variation detected by SLR is the north to south surface mass movement over Eurasia and North America, rather than the anomalously dispersive 18.6-year tide.

[56] **Acknowledgments.** This research was carried out at the Jet Propulsion Laboratory, California Institute of Technology, under a contract with NASA, and funded through NASA's Solid Earth and Natural Hazard and Cryospheric Sciences programs and the internal Research and Technology Development (R&TD) program. Partial support was also provided by Chinese National Sciences Foundation grant 49904002. We thank Ron Blom for his leadership as the PI of the R&TD strategic initiative task. Level 2 GRACE data products are provided by GRACE Science Data System through PO.DAAC. Min Zhong has pointed out an error in our earlier handling of the degree-2 GRACE data. We are grateful to Byron Tapley for his leadership and for his encouragement of our work, to Srinivas Bettadpur and John Ries of the University of Texas, Rui Ponte of AER, Chi-Fan Shih of NCAR, and Richard Gross, Michael Kelsay, Fabiano Oyafuso, Benyang Tang, Zhangfan Xing, and Dah-Ning Yuan of JPL for their efforts, help, and discussions. Tonie van Dam and an anonymous reviewer made valuable comments and suggestions that improved this manuscript. We also thank many colleagues in JPL's Tracking and Applications section and the geodetic community for their efforts in data acquisition, processing, and archive.

References

- Argus, D. F., M. B. Heflin, G. Peltzer, F. Cramp, and F. H. Webb (2005), Interseismic strain accumulation and anthropogenic motion in metropolitan Los Angeles, *J. Geophys. Res.*, *110*, B04401, doi:10.1029/2003JB002934.
- Bender, P. L., J. L. Hall, and J. Ye (2003), Satellite-satellite laser links for future gravity missions, *Space Sci. Rev.*, *108*, 377–384.
- Benjamin, D., J. Wahr, and S. Desai (2003), Earth tides, mantle anelasticity, and the post-1998 change in the Earth's oblateness, *Eos Trans. AGU*, *84*(46), Fall Meet. Suppl., Abstract G31C-05.
- Blewitt, G., and P. Clarke (2003), Inversion of Earth's changing shape to weigh sea level in static equilibrium with surface mass redistribution, *J. Geophys. Res.*, *108*(B6), 2311, doi:10.1029/2002JB002290.
- Blewitt, G., M. B. Heflin, F. H. Webb, U. J. Lindqwister, and R. P. Malla (1992), Global coordinates with centimeter accuracy in the international terrestrial reference frame using GPS, *Geophys. Res. Lett.*, *19*, 853–856.
- Blewitt, G., D. Lavallee, P. Clarke, and K. Nurutdinov (2001), A new global mode of Earth deformation: Seasonal cycle detected, *Science*, *294*, 2342–2345.
- Bouille, F., A. Cazenave, J. M. Lemoine, and J. F. Cretaux (2000), Geocenter motion from the DORIS space system and laser data on Lageos satellites: Comparison with surface loading data, *Geophys. J. Int.*, *143*, 71–82.
- Bouman, J., R. Koop, C. C. Tscherning, and P. Visser (2004), Calibration of GOCE SGG data using high-low SST, terrestrial gravity data and global gravity field models, *J. Geod.*, *78*, 124–137.
- Chambers, D. P., J. Wahr, and R. S. Nerem (2004), Preliminary observations of global ocean mass variations with GRACE, *Geophys. Res. Lett.*, *31*, L13310, doi:10.1029/2004GL020461.
- Chao, B. F. (2005), On inversion for mass distribution from global (time-variable) gravity field, *J. Geodyn.*, *39*, 223–230.
- Chen, J. L., C. R. Wilson, R. J. Eanes, and R. S. Nerem (1999), Geophysical interpretation of observed geocenter variations, *J. Geophys. Res.*, *104*, 2683–2690.
- Cheng, M., and B. D. Tapley (1999), Seasonal variations in low degree zonal harmonics of the Earth's gravity field from satellite laser ranging observations, *J. Geophys. Res.*, *104*, 2667–2681.
- Cheng, M., and B. D. Tapley (2004), Variations in the Earth's oblateness during the past 28 years, *J. Geophys. Res.*, *109*, B09402, doi:10.1029/2004JB003028.
- Cox, C. M., and B. F. Chao (2002), Detection of a large-scale mass redistribution in the terrestrial system since 1998, *Science*, *297*, 831–833.
- Demek, J. (1994), Global warming and permafrost in Eurasia: A catastrophic scenario, *Geomorphology*, *10*, 317–329.
- Dickey, J. O., S. L. Marcus, O. de Viron, and I. Fukumori (2002), Recent Earth oblateness variations: Unraveling climate and postglacial rebound effects, *Science*, *298*, 1975–1977.
- Dong, D., J. O. Dickey, Y. Chao, and M. Cheng (1997), Geocenter variations caused by atmosphere ocean and surface ground water, *Geophys. Res. Lett.*, *24*, 1867–1870.
- Eanes, R. J., S. Kar, S. V. Bettadpur, and M. M. Watkins (1997), Low-frequency geocenter motion determined from SLR tracking (abstract), *Eos Trans. AGU*, *78*(46), Fall Meet. Suppl., F146.
- Farrell, W. E. (1972), Deformation of the Earth by surface loads, *Rev. Geophys.*, *10*, 761–797.
- Fukumori, I., R. Raghunath, L. Fu, and Y. Chao (1999), Assimilation of TOPEX/Poseidon data into a global ocean circulation model: How good are the results?, *J. Geophys. Res.*, *104*, 25,647–25,665.
- Galloway, D. L., K. W. Hudnut, S. E. Ingebritsen, S. P. Phillips, G. Peltzer, F. Rogez, and P. A. Rosen (1998), Detection of aquifer system compaction and land subsidence using interferometric synthetic aperture radar, Antelope Valley, Mojave Desert, California, *Water Resour. Res.*, *34*(10), 2573–2585.
- Greatbatch, R. J. (1994), A note on the representation of steric sea level in models that conserve volume rather than mass, *J. Geophys. Res.*, *99*, 12,767–12,771.
- Gross, R. S., G. Blewitt, P. J. Clarke, and D. Lavallee (2004), Degree-2 harmonics of the Earth's mass load estimated from GPS and Earth rotation data, *Geophys. Res. Lett.*, *31*, L07601, doi:10.1029/2004GL019589.
- Heflin, M., et al. (1992), Global geodesy using GPS without fiducial sites, *Geophys. Res. Lett.*, *19*, 131–134.
- Heflin, M., D. Argus, D. Jefferson, F. Webb, and J. Zumberge (2002), Comparison of a GPS-defined global reference frame with ITRF2000, *GPS Solutions*, *6*, 72–75.
- Hughes, C. W., and V. N. Stepanov (2004), Ocean dynamics associated with rapid J_2 fluctuations: Importance of circumpolar modes and identification of a coherent Arctic mode, *J. Geophys. Res.*, *109*, C06002, doi:10.1029/2003JC002176.
- Ivins, E. R., C. G. Sammis, and C. F. Yoder (1993), Deep mantle viscous structure with prior estimate and satellite constraint, *J. Geophys. Res.*, *98*, 4579–4609.
- Kalnay, E., et al. (1996), The NCEP/NCAR 40-year reanalysis project, *Bull. Am. Meteorol. Soc.*, *77*, 437–471.
- Kusche, J., and E. J. O. Schrama (2005), Surface mass redistribution inversion from global GPS deformation and Gravity Recovery and Climate Experiment (GRACE) gravity data, *J. Geophys. Res.*, *110*, B09409, doi:10.1029/2004JB003556.
- Lambeck, K. (1988), *Geophysical Geodesy*, 718 pp., Oxford Univ. Press, New York.
- Lavallee, D., G. Blewitt, P. Clarke, and T. van Dam (2003), Seasonal variation in the spatial distribution of surface mass estimated using GPS, *Eos Trans. AGU*, *84*(46), Fall Meet. Suppl., Abstract G51C-02.

- Matsu'ura, M., and N. Hirata (1982), Generalized least-squares solutions to quasilinear inverse problems with a priori information, *J. Phys. Earth*, *30*(6), 451–468.
- Ngo-Duc, T., K. Laval, J. Polcher, and A. Cazenave (2005), Contribution of continental water to sea level variations during the 1997–1998 El Niño–Southern Oscillation event: Comparison between Atmospheric Model Intercomparison Project simulations and TOPEX/Poseidon satellite data, *J. Geophys. Res.*, *110*, D09103, doi:10.1029/2004JD004940.
- Ray, J., (Ed.) (1999), IERS Analysis Campaign to Investigate Motions of the Geocenter, *IERS Tech. Note 25*, 121 pp., Cent. Bur. of IERS, Paris.
- Ray, J., G. Gendt, R. Ferland, and Z. Altamimi (2005), Short-term instabilities in IGS coordinate frames, paper presented at 2005 EGU General Assembly, Vienna, Austria.
- Serreze, M. C., and R. G. Barry (2005), *The Arctic Climate System*, Cambridge Univ. Press, New York.
- Stammer, D., C. Wunsch, I. Fukumori, and J. Marshall (2002), State estimation in modern oceanographic research, *Eos Trans. AGU*, *83*(27), 294–295, 289.
- Tapley, B. D., S. Bettadpur, J. C. Ries, P. F. Thompson, and M. M. Watkins (2004), GRACE measurements of mass variability in the Earth system, *Science*, *305*, 503–505.
- Tregoning, P., and T. van Dam (2005), Effects of atmospheric pressure loading and seven-parameter transformations on estimates of geocenter motion and station heights from space geodetic observations, *J. Geophys. Res.*, *110*, B03408, doi:10.1029/2004JB003334.
- Trupin, A. S., M. F. Meier, and J. M. Wahr (1992), Effects of melting glaciers on the Earth's rotation and gravitational field: 1965–1984, *Geophys. J. Int.*, *108*, 1–15.
- van Dam, T. M., J. M. Wahr, Y. Chao, and E. W. Leuliette (1997), Predictions of crustal deformation and of geoid and sea-level variability caused by oceanic and atmospheric loading, *Geophys. J. Int.*, *129*(3), 507–517.
- Van der Veen, C. J. (1991), State of balance of the cryosphere, *Rev. Geophys.*, *29*, 433–455.
- Velicogna, I., J. Wahr, E. Hanna, and P. Huybrechts (2005), Short term mass variability in Greenland, from GRACE, *Geophys. Res. Lett.*, *32*, L05501, doi:10.1029/2004GL021948.
- Wahr, J. M., M. Molenaar, and F. Bryan (1998), Time variability of the Earth's gravity field: Hydrological and oceanic effects and their possible detection using GRACE, *J. Geophys. Res.*, *103*, 30,205–30,229.
- Wahr, J., S. Swenson, V. Zlotnicki, and I. Velicogna (2004), Time-variable gravity from GRACE: First results, *Geophys. Res. Lett.*, *31*, L11501, doi:10.1029/2004GL019779.
- Wilhelm, H. (1986), Spheroidal and torsional global response functions, *J. Geophys.*, *59*, 16–22.
- Wu, X., D. F. Argus, M. B. Heflin, E. R. Ivins, and F. H. Webb (2002), Site distribution and aliasing effects in the inversion for load coefficients and geocenter motion from GPS data, *Geophys. Res. Lett.*, *29*(24), 2210, doi:10.1029/2002GL016324.
- Wu, X., M. B. Heflin, E. R. Ivins, D. F. Argus, and F. H. Webb (2003), Large-scale global surface mass variations inferred from GPS measurements of load-induced deformation, *Geophys. Res. Lett.*, *30*(14), 1742, doi:10.1029/2003GL017546.
- Yamazaki, Y., J. Kubota, T. Ohata, V. Vuglinsky, and T. Mizuyama (2006), Seasonal changes in runoff characteristics on a permafrost watershed in the southern mountainous region of eastern Siberia, *Hydrol. Process.*, *20*, 453–467.
- Yoder, C. F., J. G. Williams, J. O. Dickey, B. E. Schutz, R. J. Eanes, and B. D. Tapley (1983), Secular variation of Earth's gravitational harmonic J2 coefficient from LAGEOS and nontidal acceleration of Earth rotation, *Nature*, *303*, 757–762.
- Zumberge, J., M. Heflin, D. Jefferson, M. Watkins, and F. Webb (1997), Precise point positioning for the efficient and robust analysis of GPS data from large networks, *J. Geophys. Res.*, *102*, 5005–5017.

I. Fukumori and E. R. Ivins, Jet Propulsion Laboratory, California Institute of Technology, 4800 Oak Grove Dr., MS 300-233, Pasadena, CA 91109, USA. (if@pacific.jpl.nasa.gov; eri@fryxell.jpl.nasa.gov)

M. B. Heflin, Jet Propulsion Laboratory, California Institute of Technology, 4800 Oak Grove Dr., MS 306-388, Pasadena, CA 91109, USA. (mbh@mail.jpl.nasa.gov)

X. Wu, Jet Propulsion Laboratory, California Institute of Technology, 4800 Oak Grove Dr., MS 238/600, Pasadena, CA 91109, USA. (xiaoping.wu@jpl.nasa.gov)